biophysics COLAB

Curated Preprint
v3 • February 13, 2025
Peer Review Information

Reviewed Preprint
v2 • February 13, 2025

Reviewed Preprint
v1 • January 24, 2025

ATP-release pannexin channels are gated by lysophospholipids

Erik Henze, Russell N. Burkhardt, Bennett W. Fox, Tyler J. Schwertfeger, Eric Gelsleichter, Kevin Michalski, Lydia Kramer, Margret Lenfest, Jordyn M. Boesch, Hening Lin, Frank C. Schroeder, Toshimitsu Kawate

Department of Molecular Medicine, Cornell University, Ithaca, NY 14853, USA • Boyce Thompson Institute, Cornell University, Ithaca, NY, USA • Department of Chemistry and Chemical Biology, Cornell University, Ithaca, NY, USA • Department of Clinical Sciences, College of Veterinary Medicine, Cornell University, Ithaca, NY, USA • Department of Molecular Biology and Genetics, Cornell University, Ithaca, NY, USA • Howard Hughes Medical Institute, USA

Evaluation Statement (5 February 2025)

Pannexin (Panx) channels are a family of poorly understood large-pore channels that mediate the release of substrates like ATP from cells, yet the physiological stimuli that activate these channels remain poorly understood. The preprint by Henze *et al.* describes an elegant approach wherein activity-guided fractionation of mouse liver led to the discovery that lysophospholipids (LPCs) activate Panx1 and Panx2 channels expressed in cells or reconstituted into liposomes. The authors provide evidence that LPC-mediated activation of Panx1 is involved in joint pain and that Panx1 channels are required for the established effects of LPC on inflammasome activation in monocytes, suggesting that Panx channels play a role in inflammatory pathways. Overall, this important study reports a previously unanticipated mechanism wherein LPCs directly activate Panx channels.

Biophysics Colab recommends this study to scientists investigating phospholipids, Panx channels, purinergic signalling and inflammation.

Biophysics Colab has evaluated this study as one that meets the following criteria:

- Rigorous methodology
- Transparent reporting
- Appropriate interpretation

(This evaluation refers to version 3 of this preprint, which has been revised in response to peer review of versions 1 and 2.)

Abstract

In addition to its role as cellular energy currency, adenosine triphosphate (ATP) serves as an extracellular messenger that mediates diverse cell-to-cell communication. Compelling evidence supports that ATP is released from cells through pannexins, a family of membrane proteins that form heptameric large-pore channels. However, the activation mechanisms that trigger ATP release by pannexins remain poorly understood. Here, we discover

lysophospholipids as endogenous pannexin activators, using activity-guided fractionation of mouse tissue extracts combined with untargeted metabolomics and electrophysiology. We show that lysophospholipids directly and reversibly activate pannexins in the absence of other proteins. Secretomics experiments reveal that lysophospholipid-activated pannexin 1 leads to the release of not only ATP but also other signaling metabolites, such as 5'-methylthioadenosine, which is important for immunomodulation. We also demonstrate that lysophospholipids activate endogenous pannexin 1 in human monocytes, leading to the release of IL-1β through inflammasome activation. Our results provide a connection between lipid metabolism and purinergic signaling, both of which play major roles in immune responses.

Introduction

Pannexins, a family of proteins that form heptameric large-pore channels, release signaling molecules like ATP and glutamate from both dying and living cells[1,2]. There are three subtypes (Panx1-3) that share a similar heptameric assembly with a membrane pore capable of allowing such signaling molecules to permeate[3–9]. All three subtypes of pannexins have been demonstrated to play important signaling roles in processes such as immune cell migration and differentiation, epilepsy, migraine, and chronic pain[10–13]. However, there is limited knowledge about how pannexins are activated, particularly in living cells.

In dying cells, Panx1-mediated ATP-release is important not only for depleting cellular energy and halting metabolism but also for facilitating the recruitment of white blood cells[14,15]. This so-called "find me" signaling allows phagocytes to clear billions of dying cells daily without causing unnecessary inflammation[15]. Single-channel recordings and *in vitro* reconstitution studies demonstrated that cleavage of the C-terminus by caspase during apoptotic cell death triggers Panx1-channel opening[16,17]. The prevailing mechanism involves the C-terminus blocking the pore in its closed conformation, with cleavage of this region facilitating pore unblocking to open the channel[4,18]. Cleavage of the C-terminus also induces a significant conformational rearrangement in the N-terminus, which appears to play a crucial role in channel gating[19].

In living cells, other activation stimuli for Panx1 must exist, as the C-terminus remains intact. Studies have suggested that Panx1 is activated through intracellular signaling triggered by the stimulation of structurally unrelated membrane receptors, such as G protein-coupled receptors (e.g., α1-adrenergic receptor[20]), ligand-gated ion channels (e.g., NMDA receptor[21]), and tumor necrosis factor receptors[22]. However, it remains unclear how Panx1 is activated downstream of these apparently unrelated receptors in living cells[3–6,23]. Furthermore, essentially nothing is known about the activation mechanisms of Panx2 and Panx3.

Our previous studies demonstrated that small molecules, such as probenecid[24], could reversibly activate a point mutant of Panx1 (e.g., W74A)[25]. We hypothesized that naturally occurring small molecules could trigger pannexin channel opening. To shed new light on the mechanisms of pannexin activation in living cells, we searched for potential signaling molecules that directly and reversibly activate pannexins.

Results

Panx1 and Panx2 are activated by lysophospholipids

To identify potential candidates for endogenous small molecules that regulate pannexin channel opening, we used an activity-guided fractionation approach[26]. We chose mouse liver as our source due to its involvement in diverse metabolic processes and its significantly larger size compared to other organs, making sample collection more feasible. Mouse liver extract was fractionated using reverse-phase chromatography and the fractions were tested for pannexin activation using whole-cell patch-clamp electrophysiology (Fig. 1a). The soluble fractions were excluded from this study, as the most polar fraction gave rise to strong channel activities in the absence of exogenously expressed pannexins (Supplementary Fig. 1a). To increase sensitivity of our screen, we employed a Panx1 construct that contains a Gly-Ser insertion at the N- terminus (dubbed "Panx1+GS"), which yields significantly larger currents than the wildtype channel in HEK293 cells[27]. For Panx2, we used the wildtype channel, as it gives rise to large currents in HEK293 cells. Panx3 was excluded because it failed to give rise to detectable currents, despite appreciable surface expression in mammalian tissue culture cells (Supplementary Fig. 1b).

Among the 18 metabolome fractions, two (#11 and #12) gave rise to robust and reversible currents specific to Panx1+GS or Panx2 (Supplementary Fig. 2a, b, and f). Comparative analysis by high performance liquid chromatography coupled to high-resolution mass spectrometry (HPLC-HRMS) revealed approximately 1,500 mass spectrometric features that were enriched more than 10-fold in active fractions compared to neighboring fractions that showed negligible activity. To narrow down the candidate metabolites, we pooled the active fractions and performed a second round of activity-guided fractionation. Two of the resulting fractions (#7 and #8) strongly activated both Panx1+GS and Panx2 (Supplementary Fig. 2c-e and g); comparative metabolomic analysis revealed twelve major metabolites at least 10-fold enriched in the active fractions relative to the neighboring inactive fractions (i.e., #6 and #9).

Analysis of their MS/MS fragmentation spectra and comparison with authentic standards indicated that the majority of the differential metabolites were lysolipids, including both isomers of palmitoyl-lysophosphatidylcholine (LPC-16:0), palmitoyl-lysophosphatidylethanolamine (LPE-16:0), and oleoyl-LPC (LPC-18:1), as well as an additional polyunsaturated LPC-20:3 (Fig. 1b). LPCs are known to serve diverse signaling roles, especially in inflammation[28], and exist in extracellular fluids at high micromolar concentrations[29], similar to the concentrations of these metabolites in the active fractions.

To test whether LPCs activate pannexins, we performed whole-cell patch-clamp recordings for the wildtype pannexin channels using synthetic compounds. We focused on LPC-16:0 (Fig. 1c), which is commercially available and the most abundant LPC variant in extracellular fluids[30,31]. For Panx1 we used HEK293S GnTI$^-$ cells, an HEK derivative commonly used for structural studies[32], as we observed significantly stronger currents in these cells. As for Panx2, we continued using HEK293 cells, as they exhibited lower background signals. Cell-surface-expression analysis revealed that both Panx1 and Panx2 were expressed at higher levels in GnTI$^-$ cells than in HEK293 cells, potentially contributing to both the increased sensitivity and background signal (Supplementary Fig. 1b). A robust and reversible current was observed for both Panx1 and Panx2 following stimulation with LPC-16:0 (Fig. 1d), while Panx3 and other large-pore channels—such as LRRC8A, connexin 43, and innexin 6—failed to show measurable currents under the same experimental conditions (Supplementary Fig. 1c and d).

Panx3 current was not observed in either HEK293 or GnTI$^-$ cells, despite detectable surface expression (Fig. 1e, Supplementary Fig. 1b and d). Recordings from vector-transfected cells and carbenoxolone (CBX) sensitivity confirmed that the LPC-16:0-mediated currents were specific to pannexins; Panx2 was insensitive to CBX (Fig. 1e), consistent with previous findings[33]. Importantly, extracellular ATP levels significantly increased when Panx1- or Panx2- expressing

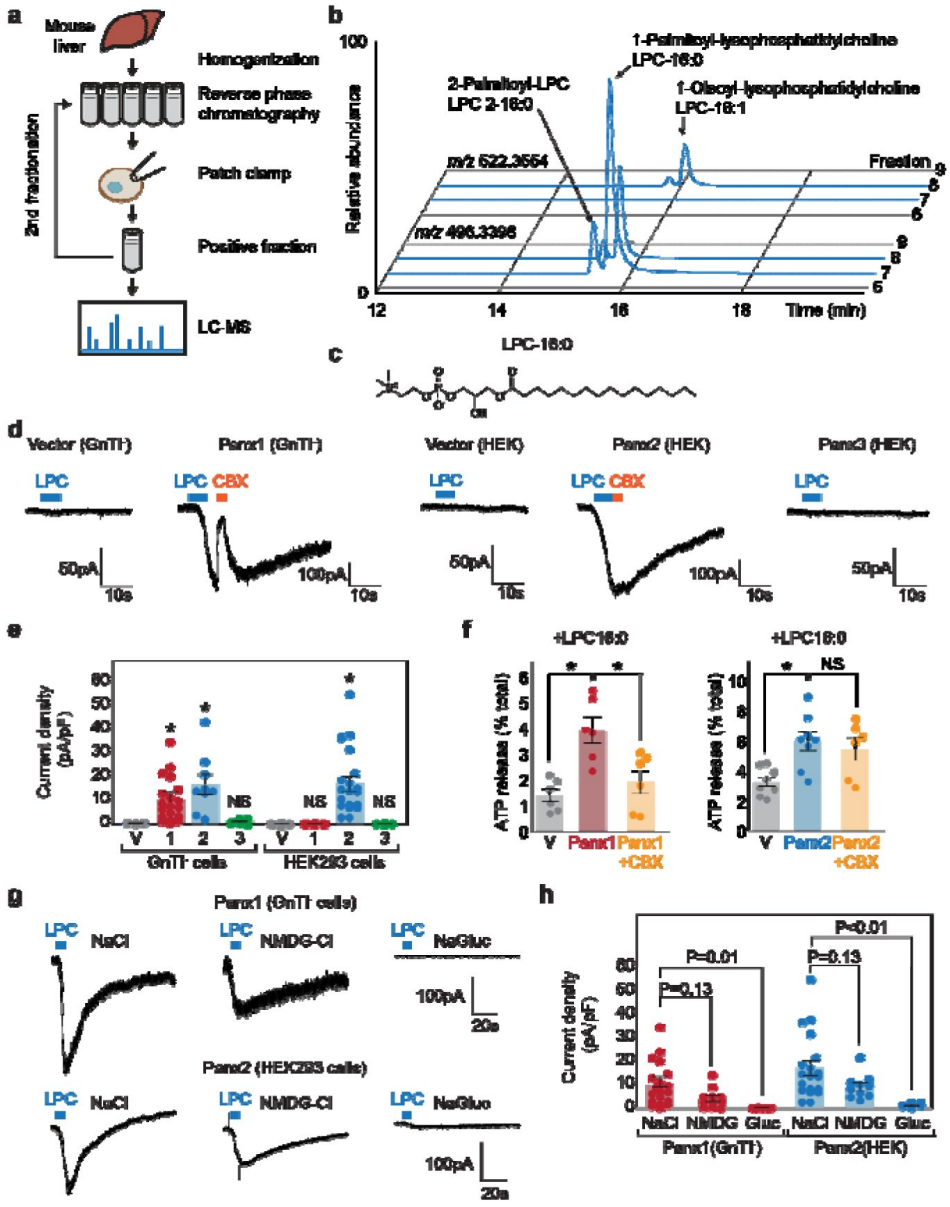

Fig. 1.

Metabolomic screening identifies LPC-16:0 as a pannexin agonist.

a Schematic of the metabolite screen. Organic extracts of mouse liver tissues were fractionated via reverse-phase chromatography and assessed for their ability to stimulate Panx1+GS or Panx2 using whole-cell patch-clamp. Active fractions were analyzed by HPLC-HRMS. **b** Extracted ion chromatograms for fractions #5-8 from the second round of Panx1 activity-guided fractionation. **c** Chemical structure of LPC-16:0. **d** Representative whole-cell patch-clamp traces. **e** Quantification of peak current densities triggered by LPC-16:0. Wildtype pannexins were expressed in indicated cells. **f** ATP release induced by application of LPC-16:0 to Panx1-expressing GnTI$^-$ (left; 10 μM at 3 min) and Panx2-expressing HEK293 (right; 30 μM at 3 min) cells. Data are expressed as percent of total ATP released upon membrane solubilization. N=6-8. P values were calculated using unpaired t-test with unequal variances. An asterisk denotes P< 0.01. Error bars represent s.e.m. **g** Representative whole cell currents of Panx1 and Panx2 stimulated by LPC-16:0 in buffers containing different anions and cations. **h** Quantification of peak current densities in different buffers. Voltage-clamp recordings were performed at -60 mV. Blue bars indicate application of LPC-16:0 (7 μM), and orange bars indicate application of carbenoxolone (50 μM). N=5-20. One-way ANOVA followed by Dunnett's test was used to assess statistical significance. V indicates the vector control.

cells were stimulated with LPC-16:0 (Fig. 1f). These results indicate that LPCs may function as endogenous signaling molecules to promote ATP-release from living cells through activation of Panx1 and/or Panx2.

To investigate the ion selectivity of lysophospholipid-activated Panx1 and Panx2 channels, we compared whole-cell current density before and after LPC treatment at -60 mV using buffers containing various anions and cations. Both Panx1 and Panx2 channels exhibited significantly larger currents in NaCl or N-Methyl-D-glucamine chloride (NMDG-Cl) compared to sodium gluconate (NaGluc), indicating that lysophospholipid-activated channels are more selective for anions under these conditions (Fig. 1g and h). This finding aligns with the reported ion selectivity of voltage-stimulated Panx1 channels[34,35]. Interestingly, currents in NMDG-Cl were slightly smaller than in NaCl, suggesting that NMDG may have an inhibitory effect on LPC- 16:0-activated channels. While we acknowledge that this analysis does not directly compare ion selectivity within the same patch, the nearly negligible current observed in NaGluc strongly indicates that the anion conductance through both Panx1 and Panx2 channels is greater than cation conductance.

We next tested structurally diverse lysophospholipids for pannexin activity. To facilitate screening, we developed a fluorescence-based assay in which iodide influx through pannexin channel is measured by fluorescence-quenching of a halide biosensor mVenus (Fig. 2a)[36,37].

This pannexin-mediated decrease in signal is normalized to the maximal quenching obtained via membrane permeabilization with the detergent, Triton-X 100. Addition of LPC-16:0 robustly quenched mVenus fluorescence in cells expressing Panx1 or Panx2 (Fig. 2b-e). Likewise, LPCs with 14:0, 18:0, 2-16:0, or 18:1 (oleoyl) acyl groups activated both Panx1 and Panx2 with EC50 values within the 10-50 μM range (Fig. 2f, g, and Supplementary Fig. 3). In contrast, neither LPC-12:0 nor LPC-20:0 activated these pannexins, suggesting that the most effective LPC acyl chain length is between 14 and 18 carbons. Lysophospholipids with other headgroups, including lysophosphatidic acid (LPA), lysophosphatidylinositol (LPI), and sphingosylphosphorylcholine (SPC) were as potent as LPC, whereas lysophosphatidylethanolamine (LPE) failed to activate pannexins even at much higher concentration (Fig. 2f, g, and Supplementary Fig. 3). Together, these results suggest that pannexins are activated by select lysophospholipids; considering that the extracellular concentrations of LPCs are orders of magnitude higher than the other tested species[30], LPCs are the most likely activators of Panx1 and Panx2 *in vivo*.

LPC-16:0 stimulation of Panx1 triggers the release of immunomodulatory metabolites

In addition to ATP, Panx1 has been demonstrated to release metabolites that play crucial roles in the resolution of inflammation and the maintenance of effector T cell populations post-infection[38,39]. We conducted comparative metabolomics to investigate whether lysophospholipids trigger the release of these or other metabolites through Panx1 channels.

GnTI$^-$ cells expressing empty vector or Panx1 were treated with vehicle or LPC-16:0, and the metabolites in the conditioned media were analyzed by HPLC-HRMS. Notably, 6 of the 25 metabolites previously identified as Panx1 permeants from apoptotic T cells[38] were enriched in the medium of Panx1-expressing cells stimulated with LPC-16:0 (Fig. 3a). These findings indicate that the selectivity of the Panx1 channel opened by lysophospholipids is comparable to the selectivity of the channel when opened by caspase-dependent C-terminal cleavage. Untargeted comparative analysis revealed additional enriched metabolites released from LPC- 16:0-stimulated Panx1-expressing cells, including the immunomodulatory metabolite 5'- methylthioadenosine (Fig. 3b and c)[40]. These data support the idea that lysophospholipids modulate inflammatory response by stimulating Panx1-dependent release of signaling metabolites beyond ATP.

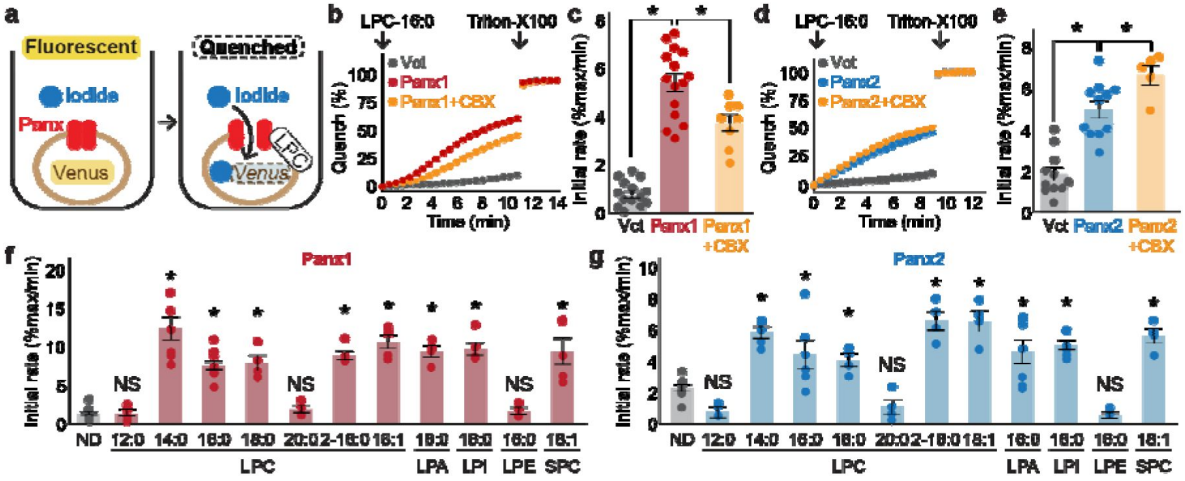

Fig. 2.

Cellular mVenus-quench assays reveal a series of lysophospholipids as pannexin agonists.

a Cartoon illustrating the principle of the mVenus quench assay. **b**-**e** Representative traces (**b** for Panx1 and **d** for Panx2) and quantification of initial mVenus quenching rates (**c** for Panx1 and **e** for Panx2). LPC-16:0 (30 μM) was applied with or without CBX (50 μM), and the maximum mVenus quenching was measured after cell solubilization with 1% Triton-X100. N=8-14. P values were calculated using unpaired t-test with unequal variances. **f** and **g** Initial mVenus quenching rates of Panx1 expressed in GnTI$^-$ cells (**f**) and Panx2 expressed in HEK293 cells (**g**). Pannexin activation was measured following addition of 60 μM sn-1 LPCs (LPC-12:0-20:0), sn-2 LPC (LPC2-16:0), a monounsaturated sn-1 (LPC-18:1), or other sn-1 lysophospholipids with different headgroups (LPA-16:0, LPI-16:0, LPE-16:0, and SPC-18:1). N=4-14. P values were calculated using one-way ANOVA followed by Dunnett's t-test. Asterisks denote P<0.01. Error bars represent s.e.m.

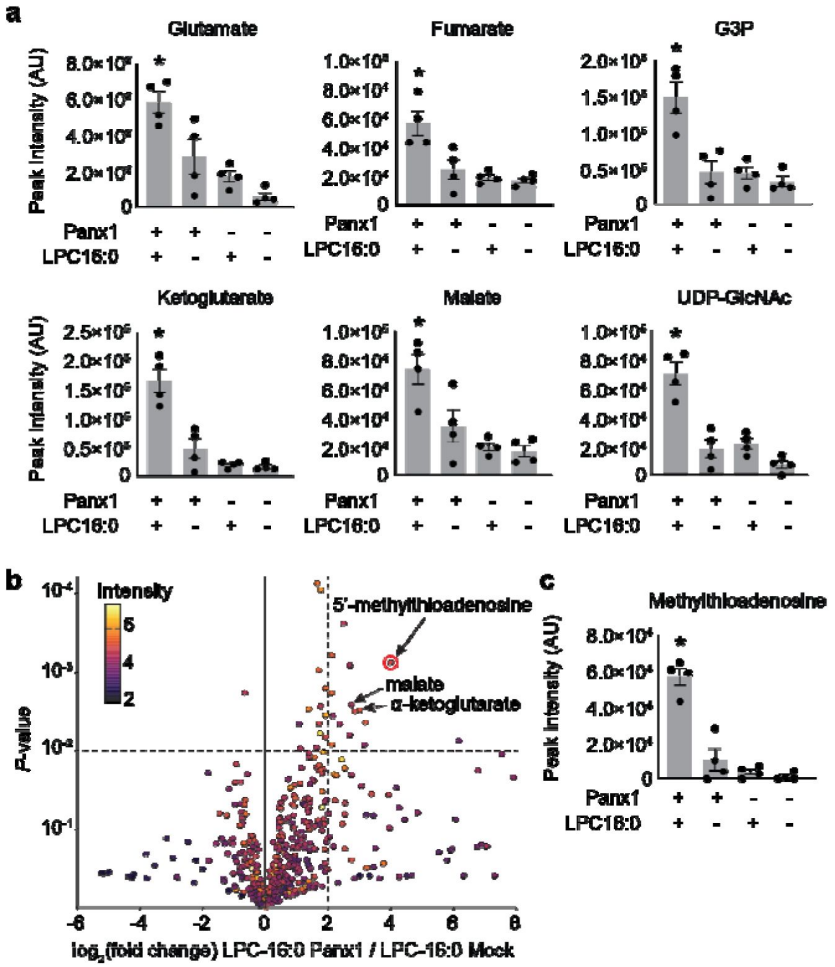

Fig. 3.

Select released signaling metabolites following LPC-16:0 stimulation of Panx1.

a Metabolites enriched in the conditioned media (CM) of cells expressing Panx1 treated with LPC-16:0 that were previously identified as Panx1 permeant using apoptotic T cells[38]. **b** Comparative analysis by HPLC-HRMS of CM from cells expressing Panx1+LPC-16:0 versus CM from vector-expressing cells treated with LPC-16:0. Volcano plot depicts subset of features detected in negative ion mode. Unadjusted *P*-values calculated by unpaired, two-sided *t*-test (see Methods for details). **c** Additional metabolite discovered in this study with known roles in immunomodulation. Panx1 was expressed in GnTI^{-} cells and the released metabolites were analyzed 45 min after the stimulation with LPC-16:0 (10 μM). N=4. P values were calculated using one-way ANOVA. Asterisks denote P<0.05. Error bars represent s.e.m.

Lysophospholipids directly activate Panx1

Evidence for several lysophospholipid-activated channels and membrane receptors[30,41,42] raises the possibility that pannexin agonism by LPC may be indirect. To test whether lysophospholipids directly activate pannexins, we performed a functional reconstitution *in vitro* to investigate pannexin activity in the absence of other proteins (Fig. 4a). The full-length Panx1 was purified from GnTI$^-$ cells using affinity and size exclusion chromatography. Purified Panx1 (Supplementary Fig. 4a and b) was reconstituted into proteoliposomes composed of 1-palmitoyl- 2-oleoyl-sn-glycero-3-phosphoethanolamine (POPE), 1-palmitoyl-2-oleoyl-sn-glycero-3-phosphoglycerol (POPG), and sphingomyelin (SM; brain extract). We assessed Panx1 channel activity through YO-PRO-1 dye uptake, a well-established method for demonstrating the activity of large-pore-forming channels using proteoliposomes[43,44]. We also confirmed that LPC-16:0 triggers YO-PRO-1 uptake in Panx1-expressing GnTI$^-$ cells using a cell-based assay (Supplementary Fig. 4c and d). Upon LPC-16:0 application, Panx1-reconstituted proteoliposomes took up YO-PRO-1 in a dose-dependent manner (Fig. 4b and c). Control proteoliposomes lacking Panx1 or CBX-treated Panx1-liposomes confirmed that the observed YO-PRO-1 uptake was Panx1 dependent. The direct effect of lysophospholipids on this channel is likely conserved across species, as we also observed LPC-16:0-dependent YO-PRO-1 uptake using proteoliposomes reconstituted with the frog Panx1 construct previously employed for cryo-EM studies[3] (Supplementary Fig. 4e-h). These results provide evidence that lysophospholipids directly activate Panx1 in the absence of other proteins.

Phospholipase A mediates pannexin activation

Lysophospholipids are produced from membrane phospholipids primarily by phospholipase A1 (PLA1) or phospholipase A2 (PLA2) enzymes[30], which hydrolyze phospholipids to produce lysophospholipids and free fatty acids important in inflammation[45] (Fig. 5a). Considering that extracellular ATP concentration increases during inflammation[46], we wondered whether phospholipase A activation may lead to increased abundance of lysophospholipids and therefore pannexin channel opening. To test this possibility, we first assessed whether extracellular application of PLA1 or sPLA2, a secreted form of this enzyme, can open pannexin channels. As with LPC-16:0, we found that application of PLA1 or sPLA2 resulted in robust mVenus quenching for both Panx1- and Panx2-expressing cells (Fig. 5b and c). Since PLA2 also leads to the production of signaling molecules other than lysophospholipids, we tested seome of these representative lipid metabolites known to mediate inflammatory responses[47].

However, none of the tested lipid species (i.e., arachidonic acid, N-arachidonoylethanolamine, prostaglandin E2, or prostaglandin I2) triggered mVenus quenching (Fig. 5d). These results suggest that lysophospholipids, but not free fatty acids or other lipid mediators, generated from the plasma membrane can activate pannexins.

We next tested whether endogenously existing cytoplasmic PLA2 (e.g., cPLA2) can activate pannexins. PLA2 is activated by polycationic amphipathic peptides commonly found in the venom of poisonous creatures. One such peptide is mastoparan, a toxic component of wasp venom that can induce cPLA2 activity in a variety of cell types[48,49]. Indeed, application of mastoparan caused a robust, CBX-sensitive mVenus quenching in cells expressing Panx1 (Fig. 5e). This quenching was attenuated by the PLA2 inhibitors chlorpromazine (CPZ) and quercetin (QCT). Because mastoparan application may trigger Panx1 activation through other mechanisms, such as C-terminal cleavage by caspase or activation of Src kinases[50], we applied mastoparan following preincubation with a pan-caspase inhibitor Z-DEVD-FMK or the Src inhibitor PP2. However, neither inhibitor affected mastoparan-dependent mVenus quenching, indicating that indirect

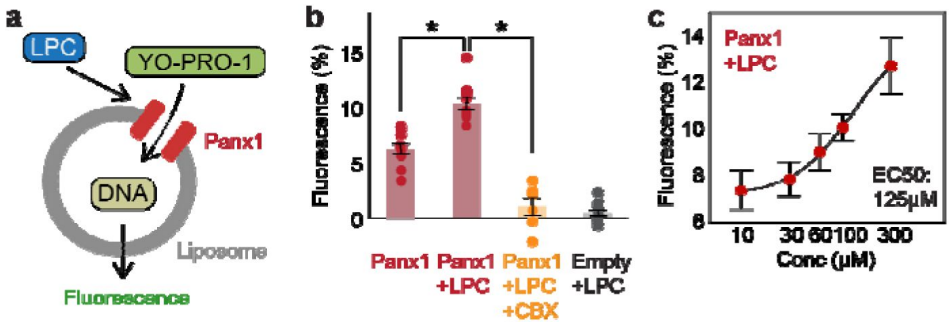

Fig. 4.

Functional reconstitution of Panx1 confirms direct activation by LPC-16:0.

a Schematic representation of YO-PRO-1 uptake assay. **b** Relative YO-PRO-1 fluorescence triggered by LPC-16:0 (100 µM) with or without CBX (50 µM). Asterisks indicate P< 0.01 using unpaired t-test. N=6-15. **c** Dose-response profile of Panx1 treated with LPC-16:0. Dose responses were fitted with the Hill equation, and the EC50 values are indicated. N=10-13. Error bars represent s.e.m.

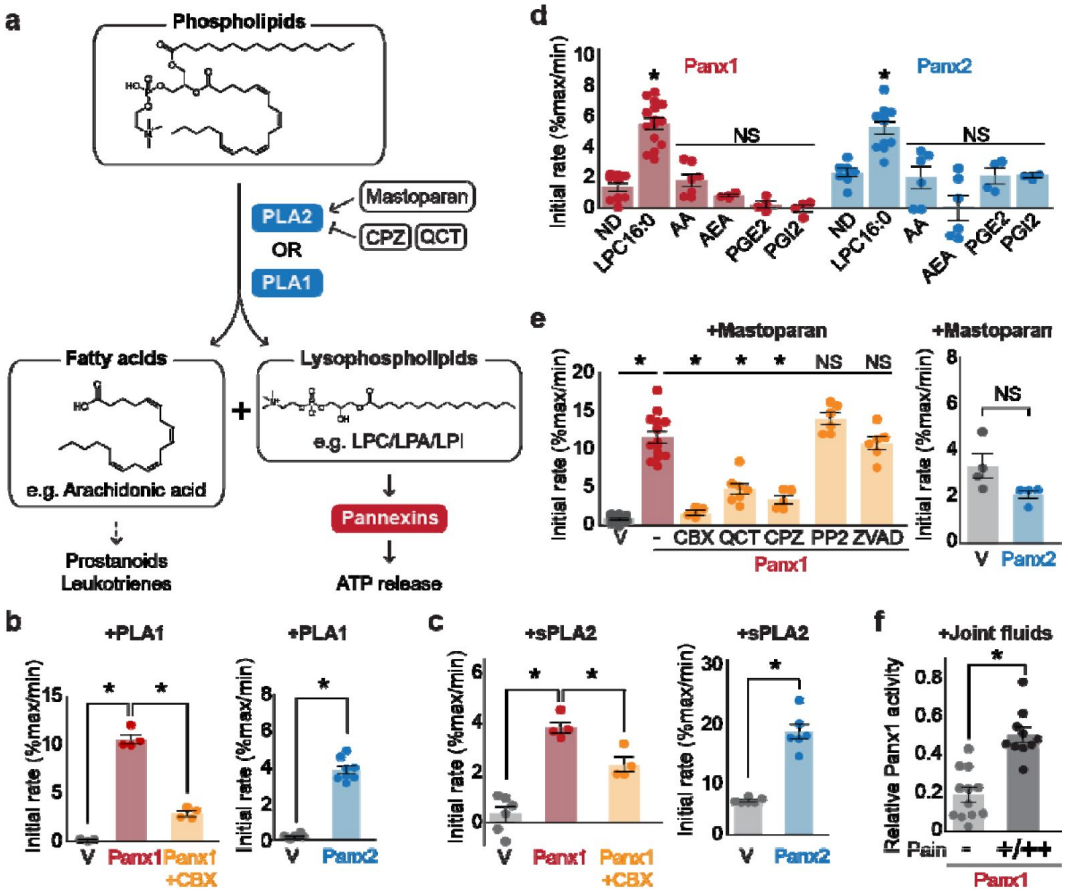

Fig. 5.

Pannexins mediate lysophospholipid signaling.

a Schematic illustrating lysophospholipid signaling. **b**-**e** Pannexin activities triggered by extracellularly applied stimuli. Normalized initial mVenus quenching rates are shown for PLA1 (**b**), sPLA2 (**c**), and major metabolic products of PLA2 (**d**), mastoparan with or without PLA2 inhibitors (QCT and CPZ), a Src kinase inhibitor (PP2), or a caspase inhibitor (ZVAD)(**e**). V indicates the vector control. Panx1 was expressed in GnTI$^-$ cells and Panx2 was expressed in HEK293 cells. N=4-14. **f** Panx1-dependent mVenus quenching induced by synovial fluids obtained from canine patients with mild (-) or moderate/severe (+/++) pain. The activity of each fraction was normalized to the effect of LPC-16:0 (30 μM). Each point represents a different patient. N=10-12. P values were calculated using unpaired Student's t-test with unequal variances (**b**, **c**, and **f**) or using one-way ANOVA, followed by Dunnett's t-test (**d** and **e**). Asterisks indicate P<0.01. Error bars represent s.e.m.

modes of Panx1 activation were unlikely (Fig. 5e). Interestingly, mastoparan-mediated mVenus quenching was not observed in cells expressing Panx2. It is possible that Panx2 may prefer lysophospholipids produced from the outer membrane leaflet.

Together, these experiments indicate that both PLA1 and PLA2 can activate pannexins, likely through the production of lysophospholipids from the plasma membrane.

Synovial fluid from canine patients experiencing pain stimulates Panx1

Given that lysophospholipid and phospholipase concentrations are elevated in patients suffering from joint diseases[51], we hypothesized that synovial fluids from dogs with naturally occurring algogenic disease might trigger Panx1 activation. To test this hypothesis, we investigated Panx1 channel activation using joint fluid collected from 22 canine patients suffering from varying degrees of pain. We found that the joint fluid collected from dogs with moderate to severe pain triggered a robust mVenus quenching (Fig. 5f). In contrast, joint fluid collected from dogs assessed to have only mild pain showed significantly weaker mVenus quenching (Fig. 5f).

These data demonstrate a correlation between pain-related behaviors and naturally occurring metabolites in synovial joint fluid that can activate Panx1.

LPC-16:0 activates endogenous Panx1 and induces the release of IL-1β from monocytes

Lysophospholipids have been demonstrated to activate the inflammasome in various cell types, including endothelial cells, microglia, and monocytes, exemplified by the cleavage and release of interlukin-1β (IL-1β)[52–55]. A recent study suggested that this mechanism relies on the P2X7 receptors, which are activated by extracellular ATP[56]. Interestingly, LPC-dependent ATP and IL-1β release were blocked by CBX or probenecid, suggesting that the release of these signaling molecules may be mediated by Panx1.

To clarify whether lysophospholipids activate endogenous Panx1 to trigger inflammasome formation, we assessed IL-1β release from phorbol 12-myristate 13-acetate (PMA)-differentiated human THP-1 monocytes. Western blot analysis confirmed the expression of endogenous Panx1 protein in PMA-differentiated THP-1 cells, and two independent shRNAs effectively reduced its expression (Fig. 6a). While lipopolysaccharide (LPS) treatment alone promoted inflammasome activation to some extent, LPC-16:0 treatment increased the amount of released cleaved IL-1β by approximately 10 fold (Fig. 6b). Panx1 cleavage was minimal and similar between the LPS-only and LPS+LPC-16:0 treated control cells, and control cells treated with LPC-16:0 alone did not promote Panx1 cleavage, indicating that the increase in IL-1β release with LPC-16:0 treatment is not due to further LPC-induced cleavage of Panx1 (Fig. 6a). Conversely, Panx1-knockdown cells released less cleaved IL-1β into the supernatant and accumulated intracellular pro-IL-1β (Fig. 6b and c). The expression levels of NLRP3 and pro-caspase 1 remained comparable among all samples, eliminating the possibility that differences in the expression levels of these key inflammasome components might explain any differences in the maturation and release of IL-1β (Supplementary Fig. 5). These findings suggest that LPC stimulation of endogenous Panx1 contributes to inflammasome activation in human monocytes.

Discussion

In this study, we demonstrate that both Panx1 and Panx2 are directly and reversibly activated by lysophospholipids at naturally occurring concentrations in body fluids produced from plasma phospholipids by PLA enzymes (Fig. 7). This *bona fide* stimulus triggers the release of signaling

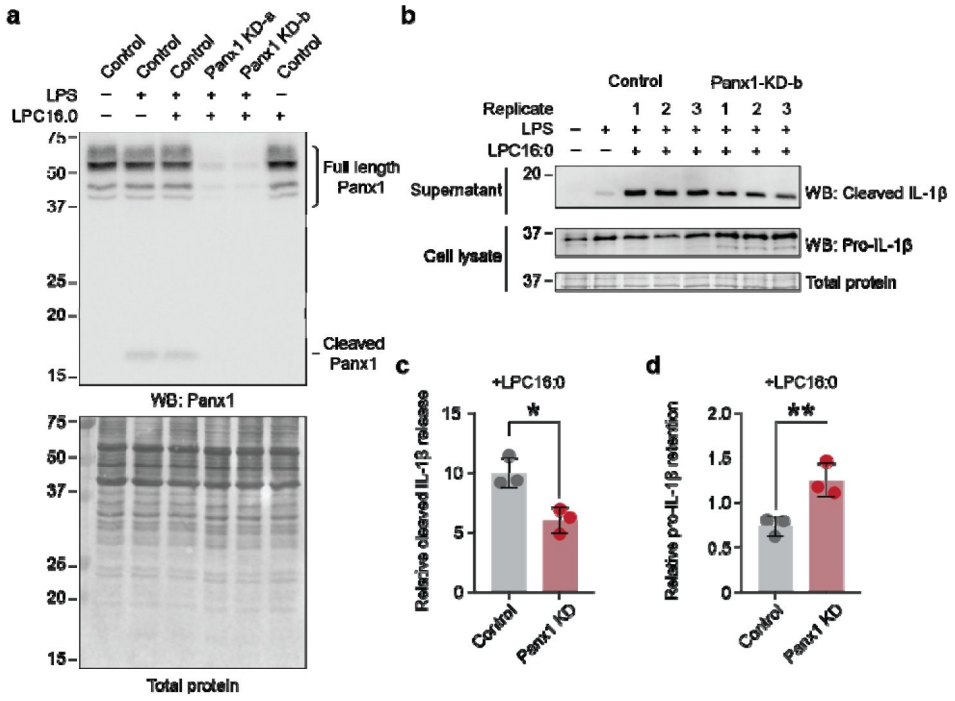

Fig. 6.

Knockdown of endogenous Panx1 reduces LPC-16:0-triggered release of cleaved IL-1β.

a Panx1 protein expression levels in PMA-differentiated/LPS-primed THP-1 control (shRNA-empty vector) cells or two different shPanx1 knockdown (KD) lines. **b** Cleaved IL-1β released into culture supernatant following stimulation with 50 μM LPC-16:0 for 1.5 h. A representative blot for control and Panx1 knockdown cells is shown. **c** Densitometry (ImageJ) was used to quantify the LPC-16:0-induced release of cleaved IL-1β from control and Panx1 KD-b cells relative to the release from control cells only primed with LPS. **d** Relative amount of the retained pro-IL-1β normalized to total protein in the cells. P values were calculated using unpaired Student's t-test. * indicates P<0.0032 and ** indicates P<0.0021. Error bars represent s.d.

molecules including ATP and the newly characterized Panx1 permeant MTA from living cells, uniting lipid and purinergic signaling pathways important for inflammation. Our *in vitro* reconstitution experiments demonstrate that full-length Panx1 can be activated by lysophospholipids in the absence of other proteins, providing compelling evidence that this channel possesses an intrinsic mechanism for activation in this manner. Considering that lysophospholipid concentrations are elevated in many inflammatory diseases[30,57], pannexin-mediated ATP release likely plays a critical role in such pathological conditions. This is consistent with our experiments demonstrating that joint fluid from dogs experiencing pain triggers robust Panx1 activation.

The discovery of lysophospholipids as a common stimulus for Panx1 and Panx2 may underlie the proposed compensatory roles between Panx1 and Panx2 described in ischemic stroke [58] and insulin secretion from β-cells[59]. Given that Panx3 is ~45% identical to Panx1 and shares a similar overall structure[7], it is surprising that Panx3 was not activated by lysophospholipids. Since Panx3 does not generate any currents in our heterologous expression systems, it is possible that Panx3 requires a currently uncharacterized posttranslational modifications or binding partners for activation by lysolipids. Alternatively, it may respond to a different class of metabolites.

Lysophospholipid-mediated pannexin activation makes biological sense for several reasons. First, PLA enzymes are activated downstream of NMDA, P2X7, TNF-α, and α1-adrenergic receptors, which have been demonstrated to lead to pannexin channel opening following their stimulation[20–22,44,60–63]. Second, the concentrations of lysophospholipids increase under pathological conditions, in which pannexins play significant roles. For example, vascular inflammation caused by platelet-derived microvesicles can be explained by the action of extracellular ATP released through Panx1 channels, as these microvesicles contain a large amount of LPCs[64]. Likewise, potentiation of angiotensin-II dependent vasoconstriction by oxidized low-density lipoproteins (oxLDLs)—a condition associated with vasospasm in atherosclerotic arteries—may be mediated by Panx1 activation, since oxLDLs are rich in LPCs[65]. Third, both augmented Panx1 channel expression and elevated levels of lysophospholipids have been independently reported to be associated with insulin resistance[28,66], a common health problem linked to a wide array of pathologic conditions, including type 2 diabetes, hypertension, and atherosclerosis.

We also demonstrated that lysophospholipids can induce the release of signaling metabolites beyond ATP through Panx1 channel activation. While it is possible that this metabolite release occurs indirectly, the overlap of several permeants with previous studies involving apoptotic T cells[38] suggests that the Panx1 channel activated by lysophospholipids in living cells likely exhibits a similar selectivity to that observed following C-terminal cleavage in dying cells. The finding of MTA as a novel Panx1-secreted metabolite opens a new area of inquiry into the role of this membrane channel in immune cell signaling, particularly as it relates to cancer[67]. MTA acts as an adenosine receptor agonist to tamp down the inflammatory response, which discourages infiltration of T cells and NK cells to the tumor microenvironment[68]. Given the emerging positive link between Panx1 expression and various cancers[69], it is possible that this metabolite is responsible for this trend.

Our findings suggest that lysophospholipids activate endogenous Panx1 in human THP- 1 cells, leading to inflammasome activation. This is consistent with a previous study demonstrating that lysophospholipids stimulate ATP release and inflammasome activation[56].

Although previous studies using bone marrow derived macrophages from Panx1-knockout mice suggested that this channel is dispensable for P2X7-dependent inflammasome activation[70], those experiments utilized both nigericin (an ionophore known to activate potassium efflux and the inflammasome) and exogenous ATP, which would directly activate the P2X7 receptor without the upstream endogenous ATP-release event. Indeed, Ismaeel et al. showed that IL-1β release was

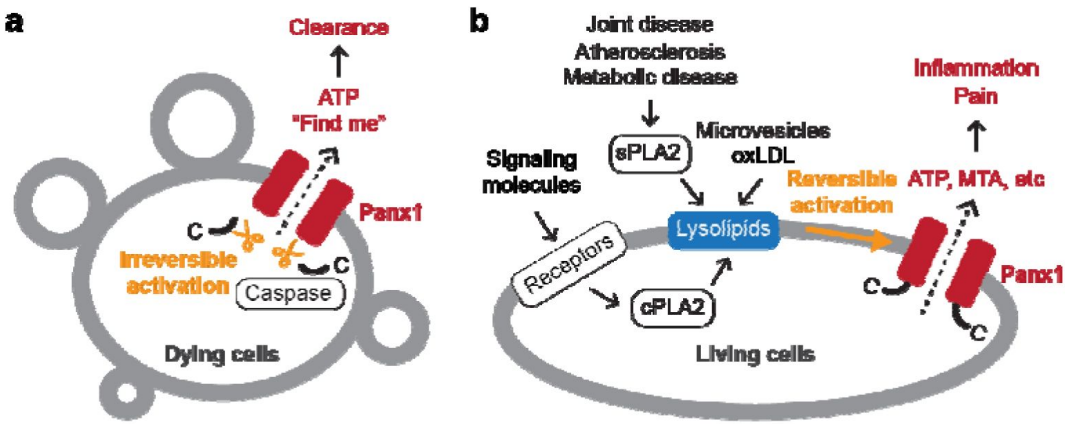

Fig. 7.

Schematic summary of Panx1-mediated signaling.

a Panx1 activation in dying cells. In dying cells, the C-terminal tails of Panx1 are cleaved by caspases, initiating an irreversible mode of Panx1 activation. This leads to the release of "find-me" signals, such as ATP, which play a role in attracting phagocytic cells to the site of cell death. **b** Panx1 activation in living cells. In living cells, activation of membrane receptors such as NMDA, P2X7, TNF-α, and α1-adrenergic receptors stimulates the production of lysophospholipids via cytoplasmic phospholipase A (PLA) enzymes. Lysophospholipids are abundant in extracellular microvesicles and oxidized low-density lipoproteins (oxLDLs). They are also produced by secreted PLAs during pathological conditions, including atherosclerosis and joint or metabolic diseases. These lysophospholipids reversibly activate Panx1, leading to the release of signaling molecules crucial for inflammation and pain.

blocked by either apyrase or P2X7 receptor antagonists[56]. Furthermore, Yang et al. showed that Panx1 was required for IL-1β release and with P2X7 exacerbated mortality in a mouse model of sepsis[71]. Interestingly, our experiments revealed that LPS stimulation alone triggered some cleavage of Panx1 and release of cleaved IL-1β to a limited extent. The limited liberation of mature IL-1β from control cells treated with LPS alone may be attributable to the Panx1-independent action of LPS on large-conductance potassium channels[72]. Nevertheless, although the underlying mechanism of Panx1 cleavage remains unclear, this cleavage may contribute to IL-1β release from cells treated only with LPS. Additionally, we observed attenuated IL-1β release in Panx1-knockdown cells; residual IL-1β release may be attributed to incomplete suppression of gene expression or through the opening of two-pore domain potassium (K2P) channels known to be involved in inflammasome activation[73–75] and activated by lysophospholipids[42].

Our functional reconstitution studies revealed some basal activity of the full-length Panx1 channel, which is inconsistent with findings from the previous study[16]. While the underlying mechanism remains unclear, there are substantial differences between the two experimental setups that may account for the divergent results. First, we used human Panx1 tagged in the flexible intracellular loop, whereas the Bayliss group used frog Panx1 tagged with GFP at the C-terminus. This difference in tagging and species may have contributed to variations in basal activity. Second, the lipid compositions used for reconstitution were significantly different. In our experiments, we used POPE, POPG, and sphingomyelin, while the Bayliss group employed a mixture of brain phosphatidylcholine, total brain lipid extract, cholesterol, and phosphatidylinositol 4,5-bisphosphate. Given that the function of many ion channels is heavily influenced by lipid composition, these differences could have contributed to the observed discrepancy. Regardless, our functional reconstitution experiments clearly demonstrate that LPC stimulates YOPRO-1 uptake in a dose-dependent manner, which forms the foundation of our interpretation.

Although our activity-guided fractionation led to the discovery of lysophospholipids as activators of Panx1 and Panx2, it is conceivable that other classes of activators may exist for these channels. Particularly, whole-cell patch-clamp experiments would limit the target molecules to those acting externally, potentially overlooking molecules that act intracellularly. Additionally, our extraction and fractionation methods were biased towards relatively non-polar compounds, leaving open the possibility that hydrophilic molecules may also activate pannexins. Nevertheless, given the signaling roles of lysophospholipids, especially in immune responses where pannexin involvement has been well-documented, it makes sense that these signaling molecules trigger the activation of pannexin channels.

In conclusion, our study supports the idea that pannexins are key downstream players in lysophospholipid signaling. Our discovery connects purinergic signaling with lipid metabolism and bolsters the importance of the less-understood lysophospholipid-mediated signaling arm of the clinically impactful lipid mediator inflammatory pathway. Alongside the well-studied activation observed in dying cells, our study unveils another layer of activation mechanisms of pannexins in living cells.

Methods

Reagents

Detergents were purchased from Anatrace and lipids were purchased from Avanti Polar Lipids. Carbenoxolone (CBX), Arachidonic acid (AA), arachidonoylethanolamide (AEA), quercetin (QCT), chlorpromazine (CPZ), PP2, biotin and desthiobiotin and were purchased from Sigma- Aldrich. Prostaglandins (PGE2, PGI2) were purchased from Abcam. Porcine pancreas sPLA2 (P6534) was purchased from Millipore Sigma. Z-DEVD-FMK (ZVAD, 210344-95-9) was purchased from Santa

Cruz Biotechnology. Mastoparan (MTP) was purchased from Santa Cruz Biotechnology (sc-200831) or Millipore Sigma (M5280). D-luciferin and luciferase were purchased from the ThermoFisher Scientifc (A22066). Lysolipids were dissolved in 100% $CHCl_3$ (Lysophosphatidylcholine (LPC) and Lysosphingomyelin (LSM)) or 70% EtOH (Lysophosphatidylinonsitol (LPI), Lysophosphatidylethanolamine (LPE), and Lysophosphatidic acid (LPA)). Solvent was evaporated under a stream of N_2 and lipids stored at -20 °C. On the day of experiments, lipids were redissolved in EtOH (LPC, LSM) or 70% EtOH(LPI, LPE, LPA) and then diluted into the indicated buffer.

Cell culture

HEK293 (CRL-1573) and HEK293S GnTI$^-$ (CRL-3022) cell lines were purchased from the American Type Culture Collection (ATCC). The mycoplasma contamination test was confirmed to be negative at ATCC and therefore were not further authenticated. HEK293 cells were maintained in Dulbecco's modified Eagle medium (ThermoFisher Scientific) supplemented with 10% FBS (Corning Life Sciences) and 10 µg/ml gentamicin (Quality Biological) at 37°C with 8% CO2 in a humidified incubator. GnTI$^-$ cells were maintained in FreeStyle 293 (ThermoFisher Scientific) supplemented with 2.5% FBS at a shaking speed of 125 rpm at 37°C with 8% CO2 in a humidified incubator. Sf9 cells (ThermoFisher Scientific) were maintained in Sf-900 III SFM (ThermoFisher Scientific) and High Five cells (ThermoFisher Scientific) cells were maintained in ESF 921 (Expression Systems) at 27°C and a shaking speed of 125 rpm. THP-1 cells (ATCC, TIB-202) were cultured in RPMI 1640 (Gibco, 11875-085) supplemented with 10% fetal bovine serum (FBS, Gibco, A52567-01, not heat-inactivated) without antibiotics and under a humidified atmosphere of 5% CO_2 at 37 °C. Cells were passed every 3-4 days, keeping their concentration to less than $1x10^6$ cells/mL. HEK293T cells were cultured in DMEM (Gibco, 11965–092) supplemented with 10% heat-inactivated calf serum (Sigma-Aldrich, C8056) without antibiotics and under a humidified atmosphere of 5% CO_2 at 37 °C. For Panx-1 shRNA stable knockdown, lentivirus was generated by co-transfection of pLKO.1 with shRNA sequences specific to pannexin-1 (TRCN0000155348 or TRCN0000154636, Millipore), psPAX2, and pMD2.G plasmids into HEK293T cells. The cell medium was collected and filtered through a 0.45-µm filter 48 h after transfection and used to infect low-passage (less than 20) THP-1 cells. After 48 h, infected cells were treated with puromycin (1 µg/mL, Goldbio) to select for stably incorporated shRNA constructs; cells were kept under selection for 3 weeks and then passed twice without puromycin before being used in experiments. Knockdown efficiency was validated by immunoblotting with pannexin-1 primary antibody (Cell Signaling Technologies, 91137, 1:1000 in 5% BSA-TBST).

Expression constructs

DNA constructs encoding the amino acid sequences of the human Panx1 (hPanx1: gene ID: 24145), frog Panx1 (frPanx1: 100170473), human Panx2 (hPanx2: 56666), human Panx3 (hPanx3: 116337), human connexin 43 (hConx43: 2697), C. elegans Inx6 (ceInx6: 178231), and human LRRC8a (hLRRC8a: 56262) were synthesized (GenScript) and subcloned using a standard molecular cloning techniques into pIE2 vector for transient expression in HEK cells, pCNG-FB7 vector for insect cell expression, or pEZT-BM (Addgene: 74099) for infecting GnTI$^-$ cells. The resulting insertion of extra residues were removed by PCR to maintain the native amino acid sequences. For pannexin western blotting, C-terminal FLAG tag was introduced by PCR. For hPanx1 purification from GnTI$^-$ cells, the flexible intracellular loop (residues 175-182) were replaced with a StrepII tag by PCR. For mVenus quenching assays, the pEZT-BM vector was modified such that the multiple cloning site is followed by the internal ribosome entry site (IRES) from encephalomyocarditis virus (EMCV) that drives the expression of mVenus (GenBank ID: AAZ65844.1; kind gift from Matt Paszek at Cornell University). To enhance the ability of iodide to quench mVenus, two point mutations (H148Q and I152L) were introduced. For cellular YO-PRO-1 uptake assays, mVenus was replaced with mCherry (GenBank ID: AY678264.1; kind gift from Hiro Furukawa at CSHL). All constructs were verified by sanger sequencing.

Whole-cell patch-clamp recordings

HEK cells or GnTI$^-$ cells (passage number < 40) were plated at low density onto 12-mm glass coverslips in wells of a six-well plate (Greiner). Cells were transfected after 24 h with ~700 ng plasmid DNA using FuGENE6 (Promega) according to the manufacturer's instructions, or infected with 5% (V/V) bacmam P2 virus. Recordings were obtained 40-60 hours after infection/transfection. Borosilicate glass pipettes (Harvard Apparatus) were pulled and heat polished to a final resistance of 2-4 MΩ and backfilled with (in mM) 147 NaCl, 10 EGTA, and 10 HEPES (adjusted to pH 7.0 with NaOH). For ion selectivity experiments, pipette solutions were identical except NaCl was replaced with NMDG-Cl or NaGluc. Patches were obtained in an external buffer containing (in mM) 147 NaCl, 2 KCl, 2 $CaCl_2$, 1 $MgCl_2$, 13 glucose, and 10 HEPES (adjusted to pH 7.3 with NaOH). For ion selectivity experiments, we exchanged external solutions before LPC-16:0 stimulation to a buffer containing NMDG-Cl (147 NMDG-Cl, 2 KCl, 2 $CaCl_2$, 1 $MgCl_2$, 13 glucose, and 10 HEPES (adjusted to pH 7.3 with NaOH)) or NaGluc ((147 NaGluc, 2 KCl, 2 $CaCl_2$, 1 $MgCl_2$, 13 glucose, and 10 HEPES (adjusted to pH 7.3 with NaOH)). A rapid solution exchange system (RSC-200; Bio-Logic) was used for recordings in which patches were perfused with drugs or mouse fractions. Currents were recorded using an Axopatch 200B patch-clamp amplifier (Axon Instruments), filtered at 2 kHz (Frequency Devices), digitized with a Digidata 1440A (Axon Instruments) with a sampling frequency of 10 kHz, and analyzed using the pCLAMP 10.5 software (Axon Instruments).

Metabolomic screening

Frozen mouse liver tissues (C57BL6J mice; 3-6 months in age; 23 females and 24 males total used in this study) were extracted in 80% MeOH using a laboratory blender on dry ice. The resulting suspension was sonicated with a microtip probe sonicator (Qsonica Ultrasonic Processor, Model Q700) for 2 minutes (2 s on/off pulse cycle) on ice at 100% power. After removing the insoluble debris by centrifugation at 5,250 RCF at 4 °C for 20 minutes, the supernatant was concentrated *in vacuo* in an SCP250EXP Speedvac Concentrator coupled to an RVT5105 Refrigerated Vapor Trap (Thermo Scientific), loaded onto Celite, and fractionated by medium pressure reverse-phase chromatography (30-gram C18 Combiflash RediSep Gold, Teledyne Isco). For the first round of fractions, an aqueous/acetonitrile solvent gradient was used at a flow rate of 20 mL/min, starting at 5% acetonitrile for 5 minutes and increasing to 100% acetonitrile over a period of 1 hr. For the second round of fractionation, the active fractions from the first round were combined and further fractionated by preparative reverse- phase chromatography using a Thermo Hypersil GOLD C18 column (10×250 mm/ 5 µm particle diameter; 25005-259070) with a 0.1% aqueous formic acid/acetonitrile gradient at a flow rate of 5 mL/min. After fractions were collected and the solvent was removed *in vacuo*, the dried fractions were stored at -20 °C. Each fraction was reconstituted in 5-25% DMSO and diluted 20-fold (first fractionation) or 300-fold (second fractionation) with the external buffer for the whole-cell patch-clamp experiments. Liquid chromatography was performed on a Thermo Vanquish Horizon HPLC system controlled by Chromeleon software (ThermoFisher Scientific) coupled to an Orbitrap Q-Exactive HF mass spectrometer controlled by Xcalibur software (ThermoFisher Scientific) outfitted with a heated electrospray ionization (HESI-II) probe. HPLC separation was achieved using a Thermo Hypersil GOLD C18 column (2.1×150 mm 1.9 µm particle size; 25002-152130) maintained at 40 °C. Solvent A: 0.1% formic acid in water; Solvent B: 0.1% formic acid in acetonitrile. A/B gradient started at 1% B for 3Lmin after injection and increased linearly to 98% B at 20Lmin, followed by 5Lmin at 98% B, then back to 1% B over 0.1Lmin and finally held at 1% B for the remaining 2.9Lmin (28Lmin total method time). Mass spectrometer parameters: spray voltage, −3.0LkV/+3.5LkV; capillary temperature 380L°C; probe heater temperature 400L°C; sheath, auxiliary, and sweep gas, 60, 20, and 2LAU, respectively; S-Lens RF level, 50; resolution, 120,000 at *m/z* 200; AGC target, 3E6. HPLC- HRMS data were analyzed using Metaboseek software with default settings after file conversion to the mzXML format via MSConvert (version 3.0, ProteoWizard)[76]. The criteria used to define a feature of interest: minimum 10-fold enrichment in the active fractions (#7 and #8) relative to neighboring fractions

(#6 and #9) and a mean intensity of 5,000,000 arbitrary units (AU) in ES+ or 2,000,000 AU in ES- for a given feature of interest in the active fractions. The resulting feature lists were manually curated to remove isotopes, adducts, and fragments, yielding twelve metabolites of interest (Table S1).

Secretomics for LPC-16:0-stimulated Panx1

HEK293 GnTI$^-$ cells were cultured on poly-D-lysine coated 6-well plates (Corning) and infected with bacmam P2 virus to induce expression of either mCherry vector alone or mCherry + Panx1. Twelve hours after the infection, 5 mM sodium butyrate was added to boost Panx1 expression and incubated for another 24 hours. Cells were washed with warmed assay buffer (147 NaCl, 10 HEPES, 13 Glucose, 2 KCl, 2 $CaCl_2$, 1 $MgCl_2$, pH 7.3 (mM)), then allowed to equilibrate in fresh assay buffer for five minutes. Cells were incubated with LPC-16:0 (final 10 μM) or an equivalent volume of assay buffer (vehicle control) for 45 minutes and the conditioned media was harvested by centrifugation at 1,000 x g for 5 min at 4°C. Conditioned media samples were lyophilized for 24-30 hours using a VirTis BenchTop 4K Freeze Dryer and then resuspended in 2 mL MeOH by vortexing and water bath sonication. The methanolic extracts were centrifuged at 4,000 x *g*, for 5 minutes at 4°C, and the resulting clarified supernatants were transferred to clean 4 mL glass vials, which were concentrated to dryness in an SC250EXP SpeedVac Concentrator coupled to an RVT5105 Refrigerated Vapor Trap (Thermo Scientific).Samples were resuspended in 0.6 mL MeOH and again concentrated to dryness as described above. Samples were finally resuspended in 70 μL MeOH, centrifuged at 4,000xg for 10min at 4°C and the clarified supernatant used for MS analysis.

Normal-phase chromatography was performed using the same system as described above. Methanolic extracts were separated on a Waters XBridge Amide column (150LmmL×L2.1Lmm, particle size 3.5 μm; Catalog no. 186004861) maintained at 40°C with a flow rate of 0.5 mL/min. Solvent A: 0.1% v/v ammonium formate in 90% acetonitrile/10% water; solvent B: 0.1% v/v ammonium formate in 30% acetonitrile/70% water. The LC method started at 1% B from 0-3 minutes, then increased linearly from 1% B to 60% B from 3-20 minutes, then increased linearly to 100% B from 20-26 minutes, followed by 5Lmin isocratic at 100% B from 26-28 minutes, then returned to 1% B isocratic from 28-31 minutes to re-equilibrate prior to the next injection.

Mass spectrometer parameters: spray voltage, -3.0 kV/+3.5LkV; capillary temperature, 380L°C; sheath gas, 60LAU; auxiliary gas, 20LAU; sweep gas, 1LAU; probe heater temperature, 400L°C; S-lens RF level 50. Full MS-SIM: resolution, 120,000 or 140,000 at *m/z* 200; AGC target, 5L×L10^6; scan range, 70-1000 m/z. Full MS/dd-MS2: MS1 resolution, 60,000 at *m/z* 200; AGC target, 3L×L10^6; Scan range, 117-1000 m/z MS2 resolution, 30,000 at m/z 200; AGC target 5e5; maximum injection time 100 ms; isolation window, 1.0 m/z; stepped normalized collision energy (NCE) 10, 30; dynamic exclusion, 3.0s; Loop count, 10.

HPLC-HRMS data were analyzed using Metaboseek software as described above. For the volcano plot in Fig. 3B, blank subtraction was performed by removing any feature less than five-fold more abundant in Panx1-expressing cells treated with LPC-16:0 relative to process blank injections. Features were further culled by removing any feature that did not have an accurate (< 5 ppm) *m/z* match to any known compound in the Human Metabolome Database[77] using the *mzMatch* feature table analysis in Metaboseek. The resulting feature list of 517 features was grouped according to treatment and analyzed by unpaired, two-sided *t*-test with no multiple testing correction. Four independent experiments were performed. Compounds reported as differential were confirmed with authentic standards using their molecular ions detected in negative electrospray ionization for quantification. In the case of methylthioadenosine, we noted significant in-source fragmentation to yield a fragment corresponding to the mass of adenine.

Cell surface biotinylation

Cell surface biotinylation, pulldown and subsequent immunoblotting were performed as described previously *(39)*. Briefly, HEK293 or HEK293 GnTI$^-$ cells were plated onto a 6-well plate and transfected using JetPrime (Polyplus) with 2.5 µg of FLAG-tagged pIE2-pannexin constructs. Two days post-transfection, cells were harvested washed in PBS. Surface membrane proteins were biotin-labeled by resuspending cells with 0.5 mg/ml sulfo-NHS-SS- biotin (Thermo Scientific) for 40 minutes at 4 °C. The reaction was quenched by washing cells twice with PBS supplemented with 50 mM NH_4Cl, followed by a final wash with 1 mL PBS. Cells were lysed in RIPA buffer (150 mM NaCl, 3 mM MgCl2, 1% NP-40, 0.5% deoxycholate (Anatrace), 0.1% SDS, 20 mM HEPES pH to 7.4 with NaOH) supplemented with 1x protease inhibitor cocktail (Thermo Scientific) and rotated for 30 minutes. The lysate was clarified by centrifugation at 21,000 x g for 15 minutes and the supernatant was recovered. Streptactin sepharose high-performance resin (GE Healthcare) was added to the lysates and rotated for 2 hours and 30 minutes. Samples were washed 6 times and the biotinylated proteins were eluted by incubating resin with 1.5 x SDS sample buffer supplemented with 75 mM DTT for 30 minutes at 55 °C with intermittent vortexing. Anti-FLAG (1:2000; clone M2), or anti-actin monoclonal antibodies (1:2000; line AC-40), were used to detect the target proteins by western blot.

Cellular pannexin activity assay

HEK293 or HEK293 GnTI$^-$ cells were plated onto 96-well poly-D-lysine coated, black-walled plates (Corning) at ~90% confluency and infected with 10% (v/v) BacMam P2 virus made with the pEZT-BM constructs encoding pannexins (and mVenus for the quench assays). Sodium butyrate (5 mM) was added to the media 10-12 hours after infection and the pannexin activity assays were performed 40-48 hours after infection (36-40 hours for hPanx1 expressed GnTI$^-$ cells). Growth media was replaced with Assay buffer containing in mM: 147 NaI (NaCl for YO- PRO-1 uptake assays), 2 $CaCl_2$, 2 KCl, 1 $MgCl_2$, 10 HEPES, 13 Glucose, pH 7.3. For the stimulation with LPA, Assay buffer was modified to include: 147 NaI, 2 KCl, 1 EGTA, 10 HEPES, 13 Glucose, pH 7.3 for preventing precipitation. After 10 minutes equilibration (for mVenus-quench) or 5 minutes equilibration with 5 µM YO-PRO-1 (for YO-PRO-1 uptake), the cells were stimulated with various compounds and enzymes as indicated in the figures. Inhibitors were added concomitantly or 5 minutes after the stimulation for sPLA2. Pannexin activity was monitored by measuring fluorescence using a plate reader (Biotek Synergy2) at 480 nm (excitation) and 528 nm (emission) wavelengths with 20 nm bandwidth. The maximum quench/fluorescence was obtained with 1% Triton-X100 or Tween-20. The percent of quenching *Q(t)* was calculated according to the following formula:

$$Q(t) = 100 * \frac{F(t) - F_i}{F_f - F_i}$$

where F_i is the initial fluorescence at 10 minutes, F_f is the final fluorescence following addition of the detergent, and *F(t)* is the fluorescence value at each time point. Each condition was tested in experimental triplicate and the resulting averaged *Q(t)* was used to obtain mVenus quenching or YO-PRPO-1 uptake rates in the initial linear range using the SLOPE function in Microsoft Excel. The dose response curves were obtained by fitting the plots with the Hill equation in Mathematica after subtracting the background fluorescence observed from the cells transfected with the vector alone.

ATP release assay

HEK293 or HEK293 GnTI$^-$ cells were plated onto poly-D-lysine coated, 96 well white-walled plates (Corning) at ~90% confluency and infected with 10% (v/v) BacMam P2 virus made with the pEZT-BM constructs encoding pannexins. Cells were washed with the external patch-clamp buffer and incubated for 10 minutes with D-luciferin (0.5 µM) and luciferase (1.3 µg/mL) using ATP

Determination Kit (ThermoFisher Scientific). Three minutes after the addition of LPC-16:0 (30 μM) in the presence or absence of CBX (50 μM), ATP released in the external buffer was measured by following the luminescence using a plate reader (Biotek Synergy2).

Luminescence was normalized to the maximum value obtained with 1% Triton-X100.

Panx1 purification

Panx1 was purified as described previously *(18)*. Briefly, Panx1 expressing cells (GnTI- for hPanx1 and HighFive cells for frPanx1-ΔLC+GS) were harvested by centrifugation and broken by nitrogen cavitation (4635 cell disruption vessel; Parr Instruments). The membrane fraction was recovered by centrifugation at 12,000 x g for 10 minutes followed by at 185,000 g for 45 minutes in PBS supplemented with a protease inhibitor cocktail (2.0 μg/mL leupeptin, 8.0 μg/mL aprotinin, 2.0 μg/mL pepstatin, and 0.5mM phenylmethylsulfonyl fluoride). Membranes were solubilized in S buffer (PBS, protease inhibitor cocktail, 10% glycerol, and 1% C12E8) for 60 minutes. Following ultracentrifugation at 185,000 x g for 45 minutes, the supernatant was incubated with Strep-Tactin Sepharose resin or Strep-Tactin XT resin (Cytiva) for 60 minutes.

The resin was washed with 10 column volumes of Wash buffer (150 mM NaCl, 100 mM Tris-HCl pH 8.0, 10% glycerol, and 0.27% C12E8) and the bound protein was eluted with 5 column volumes of Wash buffer containing 2.5 mM desthiobiotin (for Sepharose) or 25 mM biotin (for XT resin). Eluted Panx1 was further purified by size-exclusion chromatography (Superdex 200; Cytiva) in SEC buffer (150mM NaCl, 20mM Tris-HCl pH 8.0, and 0.27% C12E8). A single monodisperse Panx1 peak was collected for functional reconstitution into liposomes or into lipid nanodiscs for cryo-EM studies. All steps were carried out at 4°C or on ice.

Functional reconstitution of Panx1

Empty liposomes composed of 1-palmitoyl-2-oleoyl-sn-glycero-3-phosphoethanolamine (POPE), 1-Palmitoyl-2-oleoyl-sn-glycero-3-phosphoglycerol (POPG), and sphingomyelin (SM; brain extract) were resuspended in Reconstitution buffer (in mM; 50 Tris-HCl, 150 NaCl, 0.1 EGTA, pH 7.4) to a concentration of 10 mg/mL and extruded thirteen times through a 400 nm polycarbonate filter before use. Following incubation with 0.65% (w/v) DDM for 15 minutes, purified Panx1 was added at 50:1 (hPanx1) or at 100:1 (frPanx1-ΔLC+GS) ratio and incubated for 30 minutes. Detergents were removed by Bio-beads SM2 (Bio-rad) and 20 bp oligo DNAs (40 μM each) were incorporated by freeze-thaw and extrusion through a polycarbonate filter.

Unincorporated DNA was digested by incubating the liposomes with 0.2 mg/mL DNAse I in the presence of 5 mM $MgCl_2$ for 60 minutes, followed by centrifugation at 280,000 g for 20 minutes and resuspension in Reconstitution buffer. DNA-incorporated proteoliposomes (50 μg/well) were dispensed into 96-well Poly-D-lysine coated black-walled plates (Corning). Upon LPC- 16:0 and YO-PRO-1 (60 nM) application, Panx1 activity was monitored by measuring fluorescence using a plate reader (Biotek Synergy2) at 480 nm (excitation) and 528 nm (emission) wavelengths with 20 nm bandwidth. The maximum fluorescence was obtained with 1% Triton-X100. Quantification of Panx1 activity was performed as described above.

Canine synovial fluid sample collection

Synovial fluid was collected from 22 different client-owned dogs presenting to the Cornell University Hospital for Animals. The Cornell University Veterinary Clinical Studies Committee approved the project (#100121-16), and all the dog owners gave informed consent to use samples from their dogs. Dogs were aged 6.5 (0.67-10) years (median [range]) and consisted of neutered females (n = 13), neutered males (n = 8), and an intact male (n = 1). Represented breeds included mixed breed (n = 8), Labrador retriever (n = 5), Golden retriever (n = 2), and n = 1 each of Akita, Australian shepherd, Bernese mountain dog, Chesapeake Bay retriever, German shepherd dog,

German shorthaired pointer, and pit bull terrier. All dogs had a history of joint pain of at least 1-month duration secondary to developmental, degenerative, and/or inflammatory disease (e.g., degeneration and rupture of the cranial cruciate ligament, osteochondrosis dissecans, osteoarthritis, septic arthritis). Synoviocentesis was performed under sedation or general anesthesia for either diagnostic or therapeutic purposes (e.g., cytology, bacterial culture, or injection of pharmaceuticals [after sample collection], n = 8), or before the start of orthopedic surgery on the joint (n = 14); an aliquot was reserved for this study. Surgeries included tibial plateau-leveling osteotomy (TPLO) with (n = 6) or without (n = 3) meniscectomy, arthroscopy (n = 2), multiple procedures on one stifle joint (n = 2), or implant removal with meniscectomy (n = 1). Samples were collected from the stifle (i.e., femorotibial or knee joint, n = 17), elbow (n = 8), and shoulder (n = 4); 1 sample was collected from either the elbow or shoulder but not labeled. Using standard aseptic technique, at least 500 µL were collected into a 2.0-mL polypropylene microcentrifuge tube and frozen at -80 °C within 30 minutes. There is currently no single validated scale for grading severity of pain of all etiologies in dogs. Therefore, before anesthetic drugs were administered, and before the synovial fluid was collected, a single investigator (a veterinary anesthesiologist experienced in assessing pain in dogs, J.M.B.) used a simple descriptive scale to grade the severity of pain in the joint to be sampled; pain was assessed as mild, moderate, or severe. Clinical signs of pain included lameness, behavioral reaction upon palpation or manipulation of the joint (i.e., struggling, vocalizing), and impaired ability to perform normal activities, such as running or using stairs.

IL-1*β* release assay using THP-1 cells

IL-1β response of PMA-differentiated THP-1 cells to treatment with LPC-16:0. THP-1 cells were seeded uniformly at a density of $1x10^6$ cells per well in a 24-well plate with 1 mL 10% FBS- RPMI supplemented with phorbol 12-myristate 13-acetate (PMA, 100 ng/mL). Empty pLKO.1 vector lentivirus-transduced THP-1 cells were used as the control. After 48 h of differentiation, the media was changed to 1 mL of 10% FBS-RPMI without PMA. After 24 h of rest, the media was replaced with 0.5 mL of 10% FBS-RPMI supplemented with or without lipopolysaccharide from Escherichia coli O111:B4 (LPS, 200 ng/mL, Sigma, L2630). After 3.5 h of priming in the incubator, each well was gently washed thrice with 0.5 mL of 37 °C serum-free RPMI (SF- RPMI). Throughout the washing procedure, a 20-mM solution of LPC-16:0 (Sigma, L5254) in PBS in a polypropylene tube was incubated at 37 °C in a water bath. The 20-mM LPC-16:0 solution was removed from the water bath and vigorously vortexed, and then an aliquot was diluted in 37 °C SF-RPMI to a final concentration of 50 µM with gentle end-over-end mixing. The PBS wash buffer was aspirated from each well and gently replaced with 380 µL of the LPC- 16:0-containing media; prior to each addition, the LPC-16:0-containing media was pipetted up- and-down 3 times to minimize loss of LPC-16:0 due to its potential adsorption to the polypropylene pipette tips. The plate was placed in the incubator for 1.5 h. The supernatant media was collected and cleared of cells by centrifugation at 5000g at 4 °C for 5 min. A 100-µL aliquot of cleared supernatant was collected for each treatment group; 20 µL of 6x Laemmli buffer was added to each aliquot, which were then heated at 95 °C for 5 min. Immediately after removing the supernatant media from the wells of the plate, each well was washed once with 0.5 mL of ice-cold PBS. Cells were lysed by the addition of lysis buffer (25 mM Tris pH 8.0, 150 mM NaCl, 10% glycerol, 1% NP-40, protease inhibitor cocktail) to each well followed by shaking at 4 °C for 45 min. Total protein of the cleared (17000g, 4 °C, 20 min) cell lysates was quantified by the Bradford assay (Pierce™ Bradford Protein Assay Kit, Thermo, 23200). A 100-µL aliquot of cleared cell lysate was collected for each treatment group; 20 µL of 6x Laemmli buffer was added to each aliquot, which were then heated at 95 °C for 5 min. Media supernatants and cell lysates were analyzed by immunoblotting (12% SDS-PAGE, 200V, 50 min; block 1 h at room temperature in 5% BSA-TBST; transfer to 0.2-µM PVDF), with gel loading volume normalized to the total protein content of cell lysates to account for any potential loss of cells following the 3 cycles of PBS washing. Blots were visualized on a BioRad ChemiDoc MP instrument using chemiluminescence (Clarity Max™ Western ECL Substrate [BioRad, 1705062S] or Pierce™ ECL Western Blotting Substrate [Thermo, 32106]). The following primary antibodies were used at 1:1000 dilution at 4 °C overnight (5% BSA-TBST): Panx1 (91137, Cell Signaling Technologies [CST]),

cleaved IL-1β (83186, CST), pro-IL-1β (12242, CST), NLRP3 (15101, CST), and caspase 1 (AG-20B-0048-C100, AdipoGen). The following secondary antibodies were used at room temperature for 1 h at 1:5000 dilution (5% BSA-TBST): anti-rabbit IgG HRP-linked (7074V, CST) and anti-mouse IgG HRP-linked (7076, CST).

Supporting information

Supplementary materials

Acknowledgements

We thank O. Boudker, K. Swartz, J. Davis, A. Alouani, Biophysics Colab, and the members the Kawate labs for helpful discussions and comments for the manuscript; W. Greentree and M. Linder for providing mouse tissues; S. Webb for the help on joint fluid sample collection.

Author Contributions

Conceptualization: EH, TK; Methodology: EH, RNB, BWF, TJS, EG,JMB, HL, FCS, TK; Investigation: EH, RNB, BWF, TJS, EG, KM, LK, ML, JMB; Visualization: EH, BWF, EG, TK; Funding acquisition: JMB, HL, FCS, TK; Project administration: JMB, HL, FCS, TK; Supervision: JMB, HL, FCS, TK; Writing – original draft: EH, TK; Writing – review & editing: EH, BWF, TJS, EG, KM, JMB, HL, FCS, TK.

Competing Interest Statement

FCS is a cofounder of Ascribe Bioscience and Holoclara Inc. All other authors declare they have no competing interests.

Data sharing plan

All data are available in the main text, the Supplementary materials, or in Source data.

References

1 Syrjanen J., Michalski K., Kawate T., Furukawa H (2021) **On the molecular nature of large-pore channels** *Journal of molecular biology* **166994** https://doi.org/10.1016/j.jmb.2021.166994 | Google Scholar

2 Dahl G (2015) **ATP release through pannexon channels** *Philos Trans R Soc Lond B Biol Sci* **370** https://doi.org/10.1098/rstb.2014.0191 | Google Scholar

3 Michalski K., et al. (2020) **The cryo-EM structure of a pannexin 1 reveals unique motifs for ion selection and inhibition** *eLife* **9** https://doi.org/10.7554/eLife.54670 | Google Scholar

4 Ruan Z., Orozco I. J., Du J., Lu W (2020) **Structures of human pannexin 1 reveal ion pathways and mechanism of gating** *Nature* **584**:646–651 https://doi.org/10.1038/s41586-020-2357-y | Google Scholar

5. Deng Z., et al. (2020) **Cryo-EM structures of the ATP release channel pannexin 1** *bioRxiv* Google Scholar

6 Kuzuya M., et al. (2022) **Structures of human pannexin-1 in nanodiscs reveal gating mediated by dynamic movement of the N terminus and phospholipids** *Sci Signal* **15** https://doi.org/10.1126/scisignal.abg6941 | Google Scholar

7 Hussain N., et al. (2024) **Cryo-EM structures of pannexin 1 and 3 reveal differences among pannexin isoforms** *Nature communications* **15** https://doi.org/10.1038/s41467-024-47142-6 | Google Scholar

8 He Z., et al. (2023) **Structural and functional analysis of human pannexin 2 channel** *Nature communications* **14** https://doi.org/10.1038/s41467-023-37413-z | Google Scholar

9 Zhang H., et al. (2023) **Cryo-EM structure of human heptameric pannexin 2 channel** *Nature communications* **14** https://doi.org/10.1038/s41467-023-36861-x | Google Scholar

10 Aquilino M. S., Whyte-Fagundes P., Zoidl G., Carlen P. L (2019) **Pannexin-1 channels in epilepsy** *Neurosci Lett* **695**:71–75 https://doi.org/10.1016/j.neulet.2017.09.004 | Google Scholar

11 Munoz M. F., Griffith T. N., Contreras J. E (2021) **Mechanisms of ATP release in pain: role of pannexin and connexin channels** *Purinergic Signal* **17**:549–561 https://doi.org/10.1007/s11302-021-09822-6 | Google Scholar

12 Yeung A. K., Patil C. S., Jackson M. F (2020) **Pannexin-1 in the CNS: Emerging concepts in health and disease** *J Neurochem* **154**:468–485 https://doi.org/10.1111/jnc.15004 | Google Scholar

13 Harcha P. A., Lopez-Lopez T., Palacios A. G., Saez P. J (2021) **Pannexin Channel Regulation of Cell Migration: Focus on Immune Cells** *Front Immunol* **12** https://doi.org/10.3389/fimmu.2021.750480 | Google Scholar

14 Imamura H., et al. (2020) **Single-cell dynamics of pannexin-1-facilitated programmed ATP loss during apoptosis** *eLife* **9** https://doi.org/10.7554/eLife.61960 | Google Scholar

15 Chekeni F. B., et al. (2010) **Pannexin 1 channels mediate 'find-me' signal release and membrane permeability during apoptosis** *Nature* **467**:863–867 https://doi.org/10.1038/nature09413 | Google Scholar

16 Narahari A. K., et al. (2021) **ATP and large signaling metabolites flux through caspase-activated Pannexin 1 channels** *eLife* **10** https://doi.org/10.7554/eLife.64787 | Google Scholar

17 Chiu Y. H., et al. (2017) **A quantized mechanism for activation of pannexin channels** *Nature communications* **8** https://doi.org/10.1038/ncomms14324 | Google Scholar

18 Sandilos J. K., et al. (2012) **Pannexin 1, an ATP release channel, is activated by caspase cleavage of its pore-associated C-terminal autoinhibitory region** *J Biol Chem* **287**:11303–11311 https://doi.org/10.1074/jbc.M111.323378 | Google Scholar

19 Henze E., Ehrlich J. J., Robertson J. L., Gelsleichter E., Kawate T (2024) **The C-terminal activating domain promotes pannexin 1 channel opening** *Proc Natl Acad Sci U S A* **121**:e2411898121 https://doi.org/10.1073/pnas.2411898121 | Google Scholar

20 Billaud M., et al. (2011) **Pannexin1 regulates alpha1-adrenergic receptor- mediated vasoconstriction** *Circ Res* **109**:80–85 https://doi.org/10.1161/CIRCRESAHA.110.237594 | Google Scholar

21 Thompson R. J., et al. (2008) **Activation of pannexin-1 hemichannels augments aberrant bursting in the hippocampus** *Science* **322**:1555–1559 https://doi.org/10.1126/science.1165209 | Google Scholar

22 Maier-Begandt D., et al. (2021) **A venous-specific purinergic signaling cascade initiated by Pannexin 1 regulates TNFalpha-induced increases in endothelial permeability** *Sci Signal* **14** https://doi.org/10.1126/scisignal.aba2940 | Google Scholar

23 Ambrosi C., et al. (2010) **Pannexin1 and Pannexin2 channels show quaternary similarities to connexons and different oligomerization numbers from each other** *J Biol Chem* **285**:24420–24431 https://doi.org/10.1074/jbc.M110.115444 | Google Scholar

24 Silverman W., Locovei S., Dahl G (2008) **Probenecid, a gout remedy, inhibits pannexin 1 channels** *American journal of physiology. Cell physiology* **295**:C761–767 https://doi.org/10.1152/ajpcell.00227.2008 | Google Scholar

25 Michalski K., Kawate T (2016) **Carbenoxolone inhibits Pannexin1 channels through interactions in the first extracellular loop** *J Gen Physiol* **147**:165–174 https://doi.org/10.1085/jgp.201511505 | Google Scholar

26 Liu Z., et al. (2018) **Predator-secreted sulfolipids induce defensive responses in C. elegans** *Nature communications* **9** https://doi.org/10.1038/s41467-018-03333-6 | Google Scholar

27 Michalski K., Henze E., Nguyen P., Lynch P., Kawate T (2018) **The weak voltage dependence of pannexin 1 channels can be tuned by N-terminal modifications** *J Gen Physiol* **150**:1758–1768 https://doi.org/10.1085/jgp.201711804 | Google Scholar

28 Law S. H., et al. (2019) **An Updated Review of Lysophosphatidylcholine Metabolism in Human Diseases** *Int J Mol Sci* **20** https://doi.org/10.3390/ijms20051149 | Google Scholar

29 Psychogios N., et al. (2011) **The human serum metabolome** *PLoS One* **6**:e16957 https://doi.org/10.1371/journal.pone.0016957 | Google Scholar

30 Tan S. T., Ramesh T., Toh X. R., Nguyen L. N (2020) **Emerging roles of lysophospholipids in health and disease** *Prog Lipid Res* **80** https://doi.org/10.1016/j.plipres.2020.101068 | Google Scholar

31 Ojala P. J., Hirvonen T. E., Hermansson M., Somerharju P., Parkkinen J (2007) **Acyl chain-dependent effect of lysophosphatidylcholine on human neutrophils** *J Leukoc Biol* **82**:1501–1509 https://doi.org/10.1189/jlb.0507292 | Google Scholar

32 Reeves P. J., Callewaert N., Contreras R., Khorana H. G (2002) **Structure and function in rhodopsin: high-level expression of rhodopsin with restricted and homogeneous N-glycosylation by a tetracycline-inducible N-acetylglucosaminyltransferase I-negative HEK293S stable mammalian cell line** *Proc Natl Acad Sci U S A* **99**:13419–13424 https://doi.org/10.1073/pnas.212519299 | Google Scholar

33 Poon I. K., et al. (2014) **Unexpected link between an antibiotic, pannexin channels and apoptosis** *Nature* **507**:329–334 https://doi.org/10.1038/nature13147 | Google Scholar

34 Romanov R. A., et al. (2012) **The ATP permeability of pannexin 1 channels in a heterologous system and in mammalian taste cells is dispensable** *J Cell Sci* **125**:5514–5523 https://doi.org/10.1242/jcs.111062 | Google Scholar

35 Ma W., et al. (2012) **Pannexin 1 forms an anion-selective channel** *Pflugers Arch* **463**:585–592 https://doi.org/10.1007/s00424-012-1077-z | Google Scholar

36 Nagai T., et al. (2002) **A variant of yellow fluorescent protein with fast and efficient maturation for cell-biological applications** *Nat Biotechnol* **20**:87–90 https://doi.org/10.1038/nbt0102-87 | Google Scholar

37 Galietta L. J., Haggie P. M., Verkman A. S (2001) **Green fluorescent protein-based halide indicators with improved chloride and iodide affinities** *FEBS Lett* **499**:220–224 https://doi.org/10.1016/s0014-5793(01)02561-3 | Google Scholar

38 Medina C. B., et al. (2020) **Metabolites released from apoptotic cells act as tissue messengers** *Nature* **580**:130–135 https://doi.org/10.1038/s41586-020-2121-3 | Google Scholar

39 Vardam-Kaur T., et al. (2024) **The ATP-exporting channel Pannexin 1 promotes CD8(+) T cell effector and memory responses** *iScience* **27** https://doi.org/10.1016/j.isci.2024.110290 | Google Scholar

40 Suzzi S., et al. (2023) **N-acetylneuraminic acid links immune exhaustion and accelerated memory deficit in diet-induced obese Alzheimer's disease mouse model** *Nature communications* **14** https://doi.org/10.1038/s41467-023-36759-8 | Google Scholar

41 Marra S., et al. (2016) **Non-acidic activation of pain-related Acid-Sensing Ion Channel 3 by lipids** *Embo J* **35**:414–428 https://doi.org/10.15252/embj.201592335 | Google Scholar

42 Maingret F., Patel A. J., Lesage F., Lazdunski M., Honore E (2000) **Lysophospholipids open the two-pore domain mechano-gated K(+) channels TREK-1 and TRAAK** *J Biol Chem* **275**:10128–10133 https://doi.org/10.1074/jbc.275.14.10128 | Google Scholar

43 Karasawa A., Michalski K., Mikhelzon P., Kawate T (2017) **The P2X7 receptor forms a dye-permeable pore independent of its intracellular domain but dependent on membrane lipid composition** *eLife* **6** https://doi.org/10.7554/eLife.31186 | Google Scholar

44 Pelegrin P., Surprenant A (2006) **Pannexin-1 mediates large pore formation and interleukin- 1beta release by the ATP-gated P2X7 receptor** *Embo J* **25**:5071–5082 https://doi.org/10.1038/sj.emboj.7601378 | Google Scholar

45 Vasquez A. M., Mouchlis V. D., Dennis E. A (2018) **Review of four major distinct types of human phospholipase A2** *Adv Biol Regul* **67**:212–218 https://doi.org/10.1016/j.jbior.2017.10.009 | Google Scholar

46 Dosch M., Gerber J., Jebbawi F., Beldi G (2018) **Mechanisms of ATP Release by Inflammatory Cells** *Int J Mol Sci* **19** https://doi.org/10.3390/ijms19041222 | Google Scholar

47 Dennis E. A., Norris P. C (2015) **Eicosanoid storm in infection and inflammation** *Nat Rev Immunol* **15**:511–523 https://doi.org/10.1038/nri3859 | Google Scholar

48 Joyce-Brady M., et al. (1991) **Mechanisms of mastoparan-stimulated surfactant secretion from isolated pulmonary alveolar type 2 cells** *J Biol Chem* **266**:6859–6865 Google Scholar

49 Gil J., Higgins T., Rozengurt E (1991) **Mastoparan, a novel mitogen for Swiss 3T3 cells, stimulates pertussis toxin-sensitive arachidonic acid release without inositol phosphate accumulation** *J Cell Biol* **113**:943–950 https://doi.org/10.1083/jcb.113.4.943 | Google Scholar

50 Lohman A. W., et al. (2019) **Regulation of pannexin channels in the central nervous system by Src family kinases** *Neurosci Lett* **695**:65–70 https://doi.org/10.1016/j.neulet.2017.09.019 | Google Scholar

51 Jacquot F., et al. (2022) **Lysophosphatidylcholine 16:0 mediates chronic joint pain associated to rheumatic diseases through acid-sensing ion channel 3** *Pain* **163**:1999–2013 https://doi.org/10.1097/j.pain.0000000000002596 | Google Scholar

52 Scholz H., Eder C (2017) **Lysophosphatidylcholine activates caspase-1 in microglia via a novel pathway involving two inflammasomes** *J Neuroimmunol* **310**:107–110 https://doi.org/10.1016/j.jneuroim.2017.07.004 | Google Scholar

53 Freeman L., et al. (2017) **NLR members NLRC4 and NLRP3 mediate sterile inflammasome activation in microglia and astrocytes** *J Exp Med* **214**:1351–1370 https://doi.org/10.1084/jem.20150237 | Google Scholar

54 Correa R., et al. (2019) **Lysophosphatidylcholine Induces NLRP3 Inflammasome-Mediated Foam Cell Formation and Pyroptosis in Human Monocytes and Endothelial Cells** *Front Immunol* **10** https://doi.org/10.3389/fimmu.2019.02927 | Google Scholar

55 Rimola V., et al. (2020) **Lysophospholipids Contribute to Oxaliplatin-Induced Acute Peripheral Pain** *J Neurosci* **40**:9519–9532 https://doi.org/10.1523/JNEUROSCI.1223-20.2020 | Google Scholar

56 Ismaeel S., Qadri A (2021) **ATP Release Drives Inflammation with Lysophosphatidylcholine** *Immunohorizons* **5**:219–233 https://doi.org/10.4049/immunohorizons.2100023 | Google Scholar

57 Kano K., Aoki J., Hla T (2022) **Lysophospholipid Mediators in Health and Disease** *Annu Rev Pathol* **17**:459–483 https://doi.org/10.1146/annurev-pathol-050420-025929 | Google Scholar

58 Bargiotas P., et al. (2011) **Pannexins in ischemia-induced neurodegeneration** *Proc Natl Acad Sci U S A* **108**:20772–20777 https://doi.org/10.1073/pnas.1018262108 | Google Scholar

59 Berchtold L. A., et al. (2017) **Pannexin-2-deficiency sensitizes pancreatic beta-cells to cytokine- induced apoptosis in vitro and impairs glucose tolerance in vivo** *Mol Cell Endocrinol* **448**:108–121 https://doi.org/10.1016/j.mce.2017.04.001 | Google Scholar

60 Burch R. M., Luini A., Axelrod J (1986) **Phospholipase A2 and phospholipase C are activated by distinct GTP-binding proteins in response to alpha 1-adrenergic stimulation in FRTL5 thyroid cells** *Proc Natl Acad Sci U S A* **83**:7201–7205 https://doi.org/10.1073/pnas.83.19.7201 | Google Scholar

61 Alzola E., et al. (1998) **Activation by P2X7 agonists of two phospholipases A2 (PLA2) in ductal cells of rat submandibular gland. Coupling of the calcium-independent PLA2 with kallikrein secretion** *J Biol Chem* https://doi.org/10.1074/jbc.273.46.30208 | Google Scholar

62 Tapia-Arancibia L., Rage F., Recasens M., Pin J. P (1992) **NMDA receptor activation stimulates phospholipase A2 and somatostatin release from rat cortical neurons in primary cultures** *Eur J Pharmacol* **225**:253–262 https://doi.org/10.1016/0922-4106(92)90027-s | Google Scholar

63 Hoeck W. G., Ramesha C. S., Chang D. J., Fan N., Heller R. A (1993) **Cytoplasmic phospholipase A2 activity and gene expression are stimulated by tumor necrosis factor: dexamethasone blocks the induced synthesis** *Proc Natl Acad Sci U S A* **90**:4475–4479 https://doi.org/10.1073/pnas.90.10.4475 | Google Scholar

64 Diehl P., et al. (2019) **Lysophosphatidylcholine is a Major Component of Platelet Microvesicles Promoting Platelet Activation and Reporting Atherosclerotic Plaque Instability** *Thromb Haemost* **119**:1295–1310 https://doi.org/10.1055/s-0039-1683409 | Google Scholar

65 Galle J., et al. (2003) **Oxidized LDL and its compound lysophosphatidylcholine potentiate AngII- induced vasoconstriction by stimulation of RhoA** *J Am Soc Nephrol* **14**:1471–1479 https://doi.org/10.1097/01.asn.0000067412.18899.9b | Google Scholar

66 Tozzi M., Hansen J. B., Novak I (2020) **Pannexin-1 mediated ATP release in adipocytes is sensitive to glucose and insulin and modulates lipolysis and macrophage migration** *Acta Physiol (Oxf* **228**:e13360 https://doi.org/10.1111/apha.13360 | Google Scholar

67 Li Y., Wang Y., Wu P (2019) **5′-Methylthioadenosine and Cancer: old molecules, new understanding** *J Cancer* **10**:927–936 https://doi.org/10.7150/jca.27160 | Google Scholar

68 Jacobs B., et al. (2020) **The Oncometabolite 5′-Deoxy-5′-Methylthioadenosine Blocks Multiple Signaling Pathways of NK Cell Activation** *Front Immunol* **11** https://doi.org/10.3389/fimmu.2020.02128 | Google Scholar

69 Laird D. W., Penuela S (2021) **Pannexin biology and emerging linkages to cancer** *Trends Cancer* **7**:1119–1131 https://doi.org/10.1016/j.trecan.2021.07.002 | Google Scholar

70 Qu Y., et al. (2011) **Pannexin-1 is required for ATP release during apoptosis but not for inflammasome activation** *Journal of immunology* **186**:6553–6561 https://doi.org/10.4049/jimmunol.1100478 | Google Scholar

71 Yang D., He Y., Munoz-Planillo R., Liu Q., Nunez G (2015) **Caspase-11 Requires the Pannexin-1 Channel and the Purinergic P2X7 Pore to Mediate Pyroptosis and Endotoxic Shock** *Immunity* **43**:923–932 https://doi.org/10.1016/j.immuni.2015.10.009 | Google Scholar

72 Parzych K., et al. (2017) **Differential role of pannexin-1/ATP/P2X(7) axis in IL-1beta release by human monocytes** *Faseb J* **31**:2439–2445 https://doi.org/10.1096/fj.201600256 | Google Scholar

73 Madry C., et al. (2018) **and Interleukin-1beta Release Are Regulated by the Two-Pore Domain K(+) Channel THIK-1** *Neuron* **97**:299–312 https://doi.org/10.1016/j.neuron.2017.12.002 | Google Scholar

74 Di A., et al. (2018) **The TWIK2 Potassium Efflux Channel in Macrophages Mediates NLRP3 Inflammasome-Induced Inflammation** *Immunity* **49**:56–65 https://doi.org/10.1016/j.immuni.2018.04.032 | Google Scholar

75 Immanuel C. N., et al. (2024) **Two-pore potassium channel TREK-1 (K2P2.1) regulates NLRP3 inflammasome activity in macrophages** *Am J Physiol Lung Cell Mol Physiol* **326**:L367–L376 https://doi.org/10.1152/ajplung.00313.2023 | Google Scholar

76 Helf M. J., Fox B. W., Artyukhin A. B., Zhang Y. K., Schroeder F. C (2022) **Comparative metabolomics with Metaboseek reveals functions of a conserved fat metabolism pathway in C. elegans** *Nature communications* **13** https://doi.org/10.1038/s41467-022-28391-9 | Google Scholar

77 Wishart D. S., et al. (2022) **HMDB 5.0: the Human Metabolome Database for 2022** *Nucleic Acids Res* **50**:D622–D631 https://doi.org/10.1093/nar/gkab1062 | Google Scholar

Author information

Erik Henze[†]
Department of Molecular Medicine, Cornell University, Ithaca, NY 14853, USA

[†]Department of Cancer Biology, Dana Farber Cancer Institute, Boston, MA, USA.

Russell N. Burkhardt
Boyce Thompson Institute, Cornell University, Ithaca, NY, USA, Department of Chemistry and Chemical Biology, Cornell University, Ithaca, NY, USA

Bennett W. Fox
Boyce Thompson Institute, Cornell University, Ithaca, NY, USA, Department of Chemistry and Chemical Biology, Cornell University, Ithaca, NY, USA

Tyler J. Schwertfeger
Boyce Thompson Institute, Cornell University, Ithaca, NY, USA, Department of Chemistry and Chemical Biology, Cornell University, Ithaca, NY, USA

Eric Gelsleichter
Department of Chemistry and Chemical Biology, Cornell University, Ithaca, NY, USA

Kevin Michalski
Department of Molecular Medicine, Cornell University, Ithaca, NY 14853, USA

Lydia Kramer[‡]
Department of Molecular Medicine, Cornell University, Ithaca, NY 14853, USA

[‡]Department of Pharmacology and Molecular Sciences, Johns Hopkins University School of Medicine, Baltimore, MD, USA.

Margret Lenfest
Department of Clinical Sciences, College of Veterinary Medicine, Cornell University, Ithaca, NY, USA

Jordyn M. Boesch
Department of Clinical Sciences, College of Veterinary Medicine, Cornell University, Ithaca, NY, USA

Hening Lin[§]
Department of Chemistry and Chemical Biology, Cornell University, Ithaca, NY, USA, Department of Molecular Biology and Genetics, Cornell University, Ithaca, NY, USA, Howard Hughes Medical Institute, USA

[§]Division of the Biological Sciences, Department of Medicine and Department of Chemistry, University of Chicago, Chicago, IL, USA.

Frank C. Schroeder
Boyce Thompson Institute, Cornell University, Ithaca, NY, USA, Department of Chemistry and Chemical Biology, Cornell University, Ithaca, NY, USA

Toshimitsu Kawate
Department of Molecular Medicine, Cornell University, Ithaca, NY 14853, USA

Corresponding author: Toshimitsu Kawate Email: toshi.kawate@cornell.edu

Copyright

Authors' Response (27 January 2025)

> Revised preprint
>
> ***GENERAL ASSESSMENT***
>
> *The revised manuscript by Henze et al. presents a novel and significant contribution to the field, demonstrating that lysophospholipids (LPC) act as endogenous activators of pannexin channels. The study provides compelling evidence that LPC activation of PANX1 and PANX2 channels facilitates the release of signaling molecules critical for immune responses, particularly in the context of inflammation and inflammasome activation. The*

> *of LPC activation, is a thoughtful revision that enhances the manuscript's focus. While the authors have addressed many of the previous critiques, key mechanistic questions remain regarding channel permeability and the specificity of LPC-induced metabolite release.*
>
> ***RECOMMENDATIONS***
>
> ***Essential revisions:***
>
> 1. *While the study suggests that LPC-induced PANX1 activation results in the release of metabolites via the pannexin channel pore, no direct evidence is provided to confirm this. It is possible that the release occurs through alternative pathways or that detected metabolites are by-products of other permeating substances. Additional experiments or a more thorough discussion of these possibilities would enhance the manuscript's rigor.*

We thank the reviewers for pointing this out. While the overlap between our current study and the published secretomics studies by Medina et al. supports the direct release of these metabolites, we agree that our experiments do not rule out the possibility of an alternative pathway. We have updated the discussion to acknowledge this limitation.

> 1. *The manuscript lacks data on the ion selectivity of LPC-activated PANX1, an important aspect for understanding the channel's permeability profile. A comparison of the selectivity of LPC-induced PANX1 currents to those activated by other stimuli, such as C-terminal cleavage or depolarization, would clarify whether LPC induces a unique or comparable open state. The reviewers appreciate the technical challenges of these experiments, however, thus a more thorough discussion of the uncertainties may be appropriate.*

We agree that characterizing the channel's permeability profile is essential. However, as the reviewers noted, prolonged or repeated lysophospholipid (LPC) perfusion often destabilizes the patch, making it difficult to apply conventional reversal potential analysis. Additionally, the application of voltage ramps would inevitably activate Panx1 channels, further complicating the interpretation of the results.

As a workaround, we analysed whole-cell current density before and after LPC treatment at -60 mV using different buffers containing various anions and cations. Both Panx1 and Panx2 channels produced significantly larger currents in NaCl or NMDG-Cl compared to NaGluconate, indicating that LPC-activated channels are more selective for anions under these conditions. Interestingly, currents in NMDG-Cl were slightly smaller than in NaCl, suggesting that NMDG may have an inhibitory effect on these channels activated by LPC. While we acknowledge that this analysis does not directly compare ion selectivity within the same patch, the almost negligible current observed in NaGluconate strongly suggests that small anion conductance through both Panx1 and Panx2 channels is greater than cation conductance. We have included these findings in the new Fig. 1.

Another important aspect of Panx1 channels is their ability to allow the permeation of cationic molecules, such as YOPRO-1, when the C-terminus is cleaved. In our experiments, we demonstrate that LPC-activated full-length Panx1 channels are permeable to both anions (e.g., ATP and Cl) and cations (e.g., YOPRO-1). Although the precise mechanism underlying ion selectivity remains to be elucidated, our data support the conclusion that LPC can facilitate the release of multiple signalling molecules through full-length Panx1.

> 1. *The YO-PRO-1 uptake observed in the absence of LPC contradicts prior findings (e.g., Bayliss et al., eLife, 2021) that full-length PANX1 does not release large molecules like ATP or YO-PRO-1 under similar conditions. This discrepancy raises concerns about the interpretation of the proteoliposome experiments. Addressing this by ion selectivity experiments, or discussing differences in experimental conditions and reconstitution protocols, could provide clarity as well as strengthen the conclusions.*

We are also aware of the discrepancy and currently lack a clear understanding of the underlying mechanism. However, there are substantial differences between the two experimental setups that may account for the divergent results.

First, we used human Panx1 tagged in the flexible intracellular loop, whereas the Bayliss group used frog Panx1 tagged with GFP at the C-terminus. This difference in tagging and species may have contributed to variations in basal activity. Second, the lipid compositions used for reconstitution were significantly different. In our experiments, we used 1-palmitoyl-2-oleoyl-sn-glycero-3-phosphoethanolamine (POPE), 1-palmitoyl-2-oleoyl-sn-glycero-3-phosphoglycerol (POPG), and sphingomyelin, while the Bayliss group employed a mixture of 70% brain phosphatidylcholine, 15% total brain lipid extract, 14% cholesterol, and 1% phosphatidylinositol 4,5-bisphosphate. Given that the function of many ion channels is heavily influenced by lipid composition, these differences could have contributed to the observed discrepancy. Regardless, our functional reconstitution experiments clearly demonstrate that LPC stimulates YOPRO-1 uptake in a dose-dependent manner, which forms the foundation of our interpretation. We have included this discussion in the revised manuscript. discrepancy.

> ***Optional suggestions:***
>
> 1. *The manuscript refers to experiments conducted in human monocytes, but the actual cell line used was THP-1, a human monocytic leukemia cell line. This should be made clearer in the text to avoid confusion.*

We are confused by this comment. Our manuscript states that we used "phorbol 12-myristate 13-acetate (PMA)-differentiated human THP-1 monocytes" which should clearly indicate which cells we used in the study.

> 1. *The behavior of LPC at concentrations exceeding its Critical Micelle Concentration (CMC) (4–8 μM for 16:0 Lyso-PC) should be considered. The authors should discuss whether micelle formation affects the observed channel activation and how this might influence the interpretation of the results.*

Our dose-response experiments, shown in Supplementary Fig. 3, suggest that CMC does not appear to affect their activity. While we are eager to understand the delivery method and action mechanisms of lysophospholipids, such studies are beyond the scope of the current work.

(This is a response to peer review conducted by Biophysics Colab on version 2 of this preprint.)